NASA Reference Publication 1246

November 1990

User's Guide: Nimbus-7 Earth Radiation Budget Narrow-Field-of-View Products

Scene Radiance Tape Products, Sorting Into Angular Bins Products, and Maximum Likelihood Cloud Estimation Products

H. Lee Kyle,
Richard R. Hucek,
Brian Groveman,
and Richard Frey

NASA

NASA Reference Publication 1246

1990

User's Guide: Nimbus-7 Earth Radiation Budget Narrow-Field-of-View Products

Scene Radiance Tape Products, Sorting Into Angular Bins Products, and Maximum Likelihood Cloud Estimation Products

H. Lee Kyle
Goddard Space Flight Center
Greenbelt, Maryland

Richard R. Hucek,
Brian Groveman,
and Richard Frey
Research and Data Systems Corporation
Greenbelt, Maryland

National Aeronautics and Space Administration
Office of Management
Scientific and Technical Information Division

TABLE OF CONTENTS

TABLE OF CONTENTS (continued)

1. INTRODUCTION

The Earth Radiation Budget (ERB) parameters, derived from the Nimbus-7 scanner measurements (Jacobowitz et al., 1984a), have recently been rederived using two new and distinct algorithms. Narrow-field-of-view (NFOV) radiances can be used to estimate the total upward flux emanating from an observed region, but this is difficult because of the anisotropic nature of the radiance fields (see Taylor and Stowe, 1984, for discussion of the degree of anisotropy involved). One procedure often used is to establish average anisotropic models for the most common scenes, set up a scene identification algorithm, and then estimate the total scene irradiance from each radiance measurement. Maps are generally used to identify surface types such as ocean, land, desert, and snow, but the most difficult step is to differentiate between clear and cloudy scenes. We have used a Maximum Likelihood Cloud Estimation (MLCE) algorithm similar, but not identical, to the Earth Radiation Budget Experiment (ERBE) algorithm (Smith et al., 1986; Wielicki and Green, 1989). Because of the unique bidirectional scanning patterns used by the Nimbus-7 ERB scanner (see Figure 3-1), radiance measurements can be collected over a period of time, sorted into angular bins (SAB), and a direct angular integration performed to determine the upward flux density. This procedure needs no angle-dependent models (ADMs) or cloud-identification algorithm. However, because of the moderate measurement rate of the scanner, it does require collecting data over a longer period of time and/or area than does the MLCE procedure. The MLCE data set gives better regional and temporal resolution, while the SAB results act as an accuracy control and yield information on average bidirectional reflectance and emittance patterns.

The original Nimbus-7 ERB scanner Earth radiation budget products (Jacobowitz et al., 1984a,b) suffered from two serious problems. First, the calculated albedos were about 10% higher than the wide-field-of-view (WFOV) values (Arking and Vemury, 1984). This was apparently caused by scene identification problems that predicted too many clouds for large satellite zenith angles. Since the ERB scanner was designed to take a large percentage of its measurements at large satellite zenith angles, this was a serious problem (Vemury et al., 1984). Secondly, the Outgoing Longwave Radiation (OLR) was calculated to be some 3 W/m^2 too low because of use of incorrect sensor temperature correction coefficients in the calibration equation (Kyle et al., 1985).

The scanner took measurements from November 16, 1978 through June 20, 1980. It normally operated on a 3-day-on/1-day-off cycle; however, prior to May 1979, this schedule was frequently interrupted because of priority requirements of the other experiments on the Nimbus-7. It was found that the ERB scanner interfered with the short-lived Limb Infrared Monitor of the Stratosphere (LIMS) Experiment. Thus, prior to May 1979, there were extended periods when the scanner measurements were too sparse for accurate results to be obtained from the SAB algorithm. In late December 1978, one of the four shortwave sensors in the scanner became too noisy for accurate measurements. Thus, during daylight there are only 75% as many shortwave measurements as there are longwave ones. This compounds the data-sampling problem. As a result, only 13 months (May 1979 through May 1980) were reprocessed using the SAB and MLCE algorithms.

The first stage in the reprocessing was to take the scanner measurements from the ERB Master Archive Tapes (MATs), optimize the calibration of the radiances, sort and average them geographically into 18,630 subtarget areas (STAs), each approximately (166 km)^2, and 49 angular bins. This is done for each half orbit so that noon and midnight measurements can be treated separately. The upward hemisphere covering an STA is divided into 85 bins, but symmetry is assumed about the principle (zenith line-Sun) plane reducing the number to 49 (see Figure 2-3). These bins were chosen as an empirical compromise. They are small enough in number to allow collection of radiances for monthly integrations on individual target areas (TA) but numerous enough to allow reasonable representation of complex bidirectional reflectance patterns. They also correspond to the angular bins used in the ERBE bidirectional reflectance models (Suttles et al., 1988). These sorted, calibrated radiances are stored on scene radiance tapes (SRTs) that are used as input in producing both the SAB and MLCE products.

The data preparation is discussed in Section 2. The SAB algorithm is covered in Section 3, and the MLCE algorithm, in Section 4. The problem of estimating diurnal averages from Sun-synchronous observations is covered in Section 5. The products are discussed and compared in Section 6, while the SRT, SAB, and MLCE tapes and parameters are described in Sections 7, 8, and 9, respectively.

The data products described here can be obtained by calling or writing:

National Space Science Data Center
Code 933.4
Goddard Space Flight Center
Greenbelt, MD 20771
Telephone: (301) 286-6695
Telex: 89675 NASCOM GBLT
TWX: 7108289716
SPAN: NSSDC::REQUEST

2. DATA PREPARATION

2.1 SORTING OF SCANNER RADIANCES

As discussed in Jacobowitz et al. (1984a), the ERB instrument is equipped with four telescopes, each containing two detectors that sense the broad-band visible (0.2-4.5 μm) and infrared (4-50 μm) radiation separately. The scan rate is variable and results in a field-of-view that ranges from 90 km^2 at nadir to about 250 km^2 at the horizon. Table 2-1 gives the characteristics of these sensors. The biaxial ERB scanner has five preprogrammed scan configurations that are shown schematically in Figure 2-1 (Jacobowitz et al., 1984a). The instrument is capable of sampling approximately 80% of the Earth's viewable disc in a little under 4 minutes. During this time, about 1,700 observations of the reflected and emitted radiation are made and recorded on magnetic tape. The instantaneous radiances and their corresponding Earth locations and geometry are available from the National Space Science Data Center (NSSDC) of the National Aeronautics and Space Administration (NASA). Each of these MATs contain 3 days of ERB data.

Table 2-1. Characteristics of ERB Scanning Channels

Channel	Wavelength Limits (μm)	Filter	Noise Equivalent Radiance (W cm^{-2}sr^{-1})	NEP (W Hz$^{-1/2}$)	FOV (°)
15-18	0.2 - 4.8	Suprasil W	3.7×10^{-5}	6.65×10^{-9}	0.25 x 5.12
19-22	4.5 - 50	Deposited layers on diamond substrate	1.8×10^{-5}	1.73×10^{-9}	0.25 x 5.12

The scan patterns 1, 2, 3, and 4 were designed to give a maximum number of angular independent views of the same geographic area, while scan pattern 5 consists of a composite of mode 3 and 4. The operating schedule of the ERB scanner is shown in Table 2-2. The scanner operated in scan mode 5 during February 1979, part of March 1979, and continuously from May through August 1979. In mid-September 1979, mode 5 failed. The scanner refused to automatically switch from mode 3 to mode 4 and back again. From then until the failure of the instrument on June 22, 1980, the scanner operated on 3 days in scan mode 3, off 1 day, and followed by 3 days on in mode 4. The operating schedule of the ERB instrument was routinely 3-days on and 1-day off with only minor interruptions resulting in 21 to 24 days of observations during a month. However, not long after the start of ERB operations it was discovered that the scanning operation was causing perturbations in the spacecraft attitude that were above the tolerance levels of the LIMS. Since the LIMS experiment was expected to have a lifetime of approximately 6 months, the ERB scanner had to compromise (Jacobowitz et al., 1984b). From mid-December 1978 through mid-April 1979, the scanner operated for only 10 to 15 days per month. In addition, during a special LIMS observation period that lasted from January 4, 1979

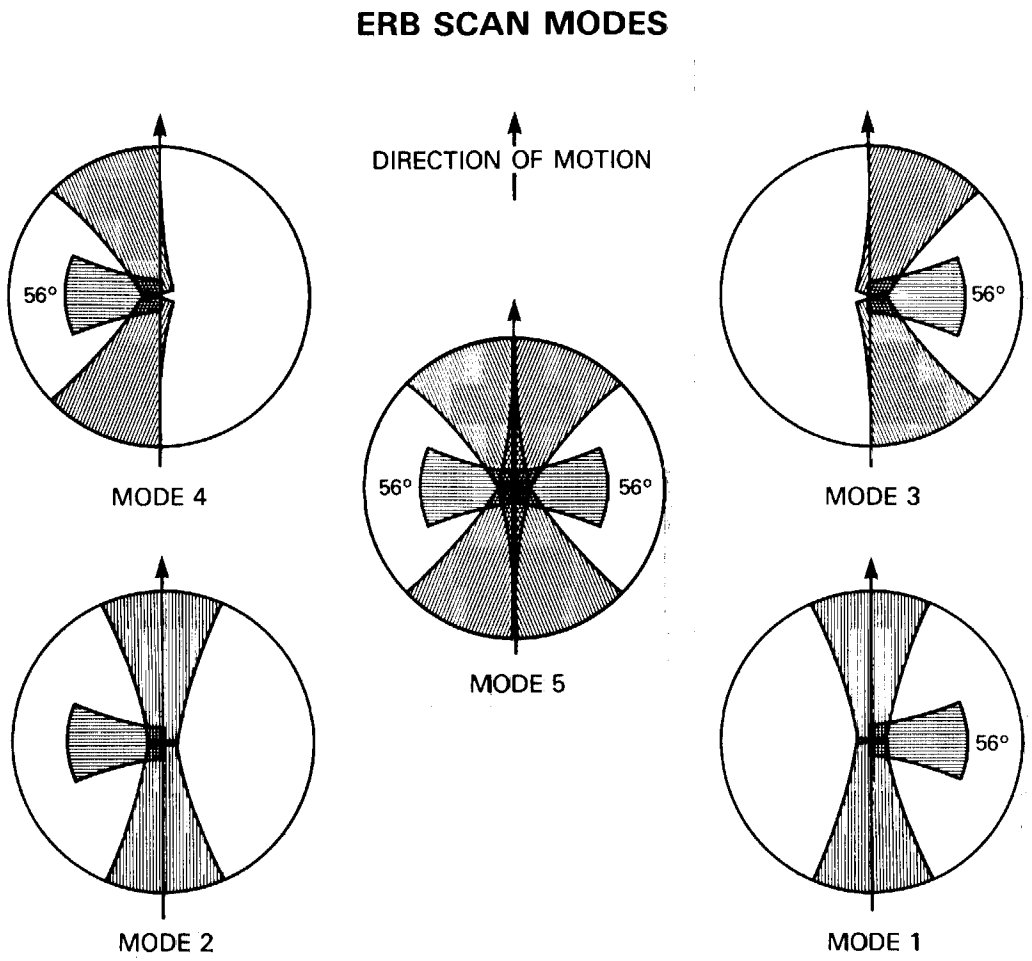

Figure 2-1. The Five ERB Scan Modes.

Table 2-2. ERB-7 Scanner Status: 1978 to 1980

	# Days Scanner On	# Days ERB Scanning	SCAN MODES					Nadir	# Days Multiple Scan Modes
			1	2	3	4	5		
DATE OF MONTH: 1-15									
November 1978									
December	11	9			9*			2	
January 1979	11	7			7*			4	
February	9	6				1	5	3	
March	11	8	1	2			4	3	1
April	9	2	2					7	
May	11	8					8	3	
June	11	11					11		
July	11	11					11		
August	11	11					11		
September	11	11	3			3	5		
October	11	10			5	5		1	
November	11	11			5	6			
December	11	11			7	4			
January 1980	11	11			5	6			
February	11	11			6	5			
March	11	11			5	6			
April	10	10			5	5			
May	12	12			6	6			
June	11	11			6	5			
DATE OF MONTH: 16-31									
November 1978	12	12			10*		1		1
December	12	8			8*			4	
January 1979	10	8			8*			2	
February	9	4					4	5	
March	12	8	4	4				4	
April	12	10	8	2				2	
May	11	11					11		
June	12	12					12		
July	12	12					12		
August	12	12					12		
September	12	11			6	5		1	
October	12	10			5	5		2	
November	11	11			5	6			
December	11	11			4	7			
January 1980	12	12			6	6			
February	11	11			6	5			
March	12	12			6	6			
April	11	11			5	6			
May	12	12			6	6			
June	4	4			3	1			
NFOV MONTHLY TOTALS	427	384	18	8	144	105	107	43	2

*Scanner alternates between modes 3 and 4 each day.

to February 6, 1979, the ERB scanning channels were forced to operate in a nadir mode at night when the satellite passed over the latitudes 80°N to 27°S (Jacobowitz et al., 1984b). As a result of these sampling constraints and instrument compromises, we have chosen to concentrate on the period from May 1979 to May 1980.

Further processing of the scanner radiances and their Earth-viewing locations from the ERB MATs has been done at the Space Data and Computing Division at NASA on an IBM 3081 computer. Each pair of radiances (reflected and emitted) is located into one of 18,630 regions (referred to as an ERB STA of approximately 166 km^2 into which the entire Earth is divided. The size of an STA varies from 1.5° latitude and longitude near the equator to 1.5° latitude and 40° longitude at the poles in order to maintain an equal area projection on the Earth. The final top of the atmosphere (TOA) Earth radiation budget averages are typically produced on approximately a 500-km^2 grid. These regions (2,070) are each composed of 9 STAs and are referred to as ERB TA. The TA world grid is described in Table 2-3 and illustrated in Figure 2-2. An STA consists of a further breakdown of each TA into 9 equal regions (1.5° latitude/longitude at the Equator). These form a 3 by 3 grid in the TA and are coded with an index ranging from 1 to 9, starting in the SE corner and ending in the NW corner as shown below.

TA

9	8	7
6	5	4
3	2	1

↑ N

The viewing geometry is sorted into 49 discrete angular bins, which are shown in Figure 2-3. The observations made between relative azimuth angles from 189° to 351° are averaged together with their symmetric counterpart on the opposite side of the plane of the Sun. The radiances, in pairs when available, are each identified with (1) the ERB TA number and STA number within the TA corresponding to the Earth location of the observation, (2) the solar zenith angle (0° at zenith), and (3) the satellite zenith angle and the relative azimuth angle measured clockwise from the Sun direction. The observed satellite zenith and relative azimuth angles are first sorted into a discrete angular bin according to the scheme described in Figure 2-3. All reflected and emitted radiances falling into each STA and each angular bin during each half-orbit (the ascending and descending nodes are each processed separately) are then averaged. The total number of STA scenes observed by the scanner during an orbit (ascending and descending nodes combined) is a function of the scan mode and ranges from 4 to 6 thousand.

Table 2-3. ERB Scanning Channel Target Areas

No. of Target Areas in Latitude Band	Sequential Target No.		Latitude Limits		Longitude Interval*
	Southern Hemisphere	Northern Hemisphere	Lower Limit	Upper Limit	
80	956-1035	1036-1115	0.0	4.5	4.5
80	876-955	1116-1195	4.5	9.0	4.5
80	796-875	1196-1275	9.0	13.5	4.5
80	716-795	1276-1355	13.5	18.0	4.5
72	644-715	1356-1427	18.0	22.5	5.0
72	572-643	1428-1499	22.5	27.0	5.0
72	500-571	1500-1571	27.0	31.5	5.0
72	428-499	1572-1643	31.5	36.0	5.0
60	368-427	1644-1703	36.0	40.5	6.0
60	308-367	1704-1763	40.5	45.0	6.0
60	248-307	1764-1823	45.0	49.5	6.0
48	200-247	1824-1871	49.5	54.0	7.5
45	155-199	1872-1916	54.0	58.5	8.0
40	115-154	1917-1956	58.5	63.0	9.0
36	79-114	1957-1992	63.0	67.5	10.0
30	49-78	1993-2022	67.5	72.0	12.0
20	29-48	2023-2042	72.0	76.5	18.0
16	13-28	2043-2058	76.5	81.0	22.5
09	4-12	2059-2067	81.0	85.5	40.0
03	1-3	2068-2070	85.5	Pole	120.0

*For each latitude band, the longitude intervals start at the 0° meridian and progress west by the increments listed.

The sequential numbering system assigns a number, between 1 and 2,070, to each target area, starting from the south pole. Within each latitude belt the numbers increase westward from the 0° meridian and continue to increase within the adjacent latitude belt to the north.

In each hemisphere, there will be 1,035 target areas and each of those areas is further divided into 9 subdivisions.

The mean number of angular views for an STA scene ranges from 3 to 5 (see Table 2-4). As expected, there is better spatial coverage with scan mode 5 at the expense of viewing fewer angular bins. The number of samples, the radiance means and their variation, along with other ancillary data, are then written to magnetic tape for all STAs that were viewed by the scanner during an orbit. These tapes are capable of storing the binned radiance averages for up to eight days of data. This results in 3 tapes per month of observations and a total of 39 tapes for the period from May 1979 to May 1980. These tapes, referred to as the ERB NFOV Scene-Radiance Tapes, are available, along with additional documentation from the NSSDC (see Section 1).

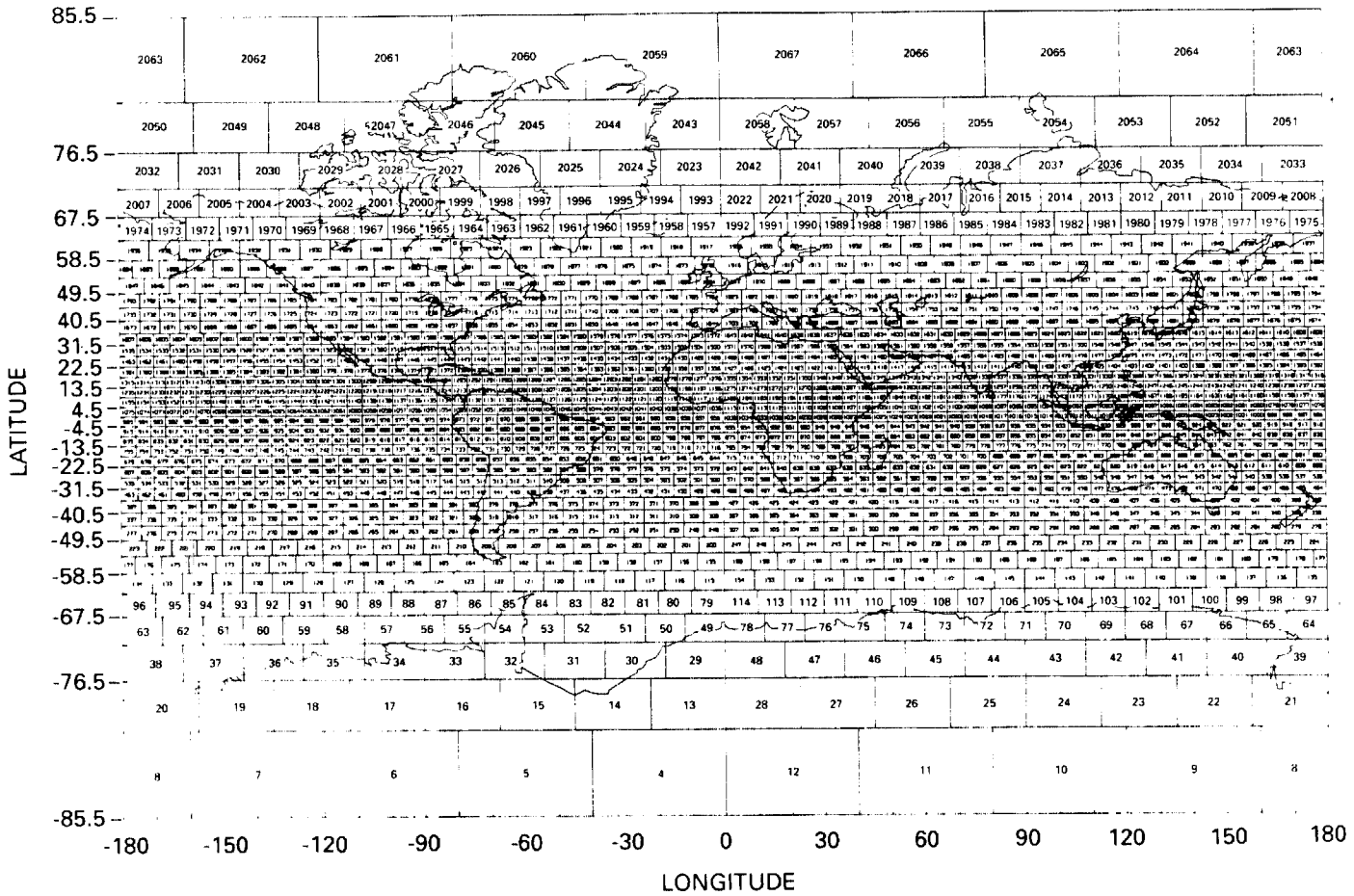

Figure 2-2. The Nimbus-7 ERB world grid of 2,070 approximately equal size TAs which are numbered consecutively from the South Pole. In each zone, the numbers increase westward from the Greenwich Meridian. The Poles are not shown.

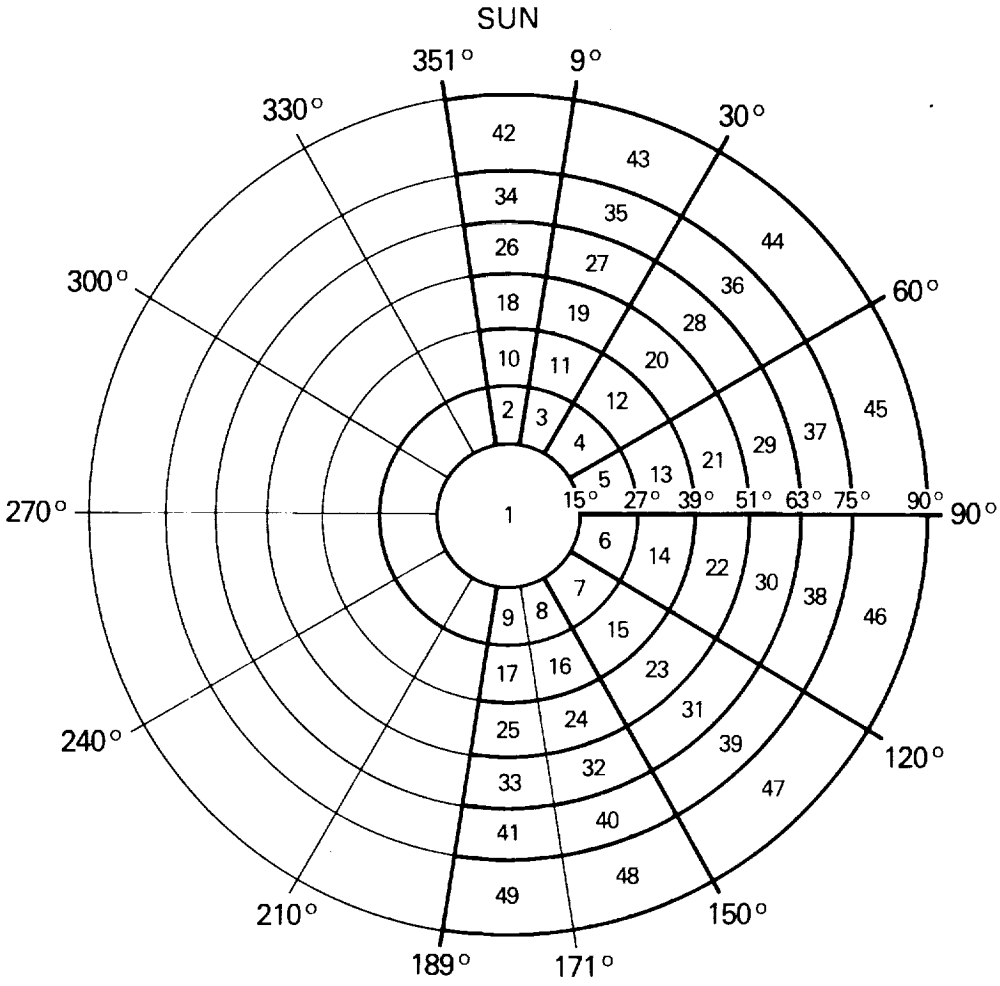

Figure 2-3. Arrangement of the 49 angular bins used for the Nimbus-7 ERB scene radiance tape. The satellite zenith angle is shown along the horizontal axis, and its azimuth angle, around the circumference.

Table 2-4. Average Number of STA Scenes and Angular Bins Observed per Orbit by the Scanner as a Function of Scan Mode

		Number of Angular Bins	
ERB Scan Mode	Number of Scenes	Mean	Standard Deviation
1/2	5000	4.2	3.5
3/4	4100	4.9	3.3
5	6250	3.4	2.5
Nadir	1100	1.1	0.3

2.2 CALIBRATION ADJUSTMENTS

2.2.1 Shortwave Scan Channels

The shortwave scan channels were calibrated in the laboratory by viewing a diffuse target, using several methods (Jacobowitz et al., 1984a). The information obtained from these preflight tests was then used for the initial calibration of the in-flight measurements. Additional postlaunch checks on the shortwave scan channels were made by comparing the observed brightness levels of nearly isotropic surfaces (i.e., cloud-free snow) to published ground-based observations, comparing the mean shortwave flux obtained from the scan channel radiances to the flux obtained from the difference between the WFOV total-spectral channel 12 and the integrated longwave scan channels over a 2-week period, and comparison of channel sensitivities obtained from views of an on-board diffuse target illuminated by the Sun with prelaunch values. These postflight calibration checks all indicated an increase in the shortwave channel sensitivity since launch (see Table 5 of Jacobowitz et al., 1984a). Additionally, it was discovered that one of the shortwave scan channels (18) became extremely noisy by the end of 1978 (Jacobowitz et al., 1984a). Consequently, we have chosen to use only the remaining three shortwave scan channels (15-17) in our analysis. The differences in the pre and postlaunch sensitivities suggested by Jacobowitz et al. (1984) have been used to adjust the shortwave radiances obtained from the ERB MAT product. Each shortwave radiance was adjusted by the appropriate factor shown in Table 2-5.

2.2.2 Longwave Scan Channels

The sensitivity and offset for the longwave scanning channels were periodically checked in flight by observing a calibration blackbody and cold space. According to Jacobowitz et al. (1984a), the deviations of the in-flight sensitivities and offsets remained constant to within $\pm 1\%$ of their initial values (see their Figures 12 and 13). A later review of the longwave scan channel calibration revealed that a slightly incorrect temperature coefficient was used in the count-conversion equation leading to the longwave radiances on the ERB MAT (Kyle et al., 1985). The magnitude of this error was determined to be about 1 $Wm^{-2}sr^{-1}$ and to be a function of the scanning channel module temperature and the digital counts. An approximate correction for this error has been determined as a function of the module temperature and digital counts over the range of expected values (Ardanuy, 1986, personal communication). The correction is in the

form of an offset to the channel 19-22 longwave radiances available on the ERB MAT. The offsets used to adjust the MAT radiances were derived from the data in Table 2-6.

The corrections provided in Table 2-6 were then used to describe the variation of the correction for the full range of observed temperatures and digital counts. This was achieved by fitting a cubic spline polynomial to the prescribed values. A two-dimensional look-up table in temperature and counts was set-up to provide an additive correction to each longwave scanner radiance as they were processed from the ERB MAT.

Table 2-5. Sensitivity Correction Made to ERB Shortwave Scan Channels Obtained from the ERB MAT

Channel	Sensitivity Correction
15	0.91
16	0.87
17	0.92
18[a]	0.83

[a]Channel 18 was not actually processed.

Table 2-6. Longwave Scan Channel Radiance Offset Correction as a Function of the Module Temperature and Digital Counts[a]

Longwave Radiance Correction ($wm^{-2}sr^{-1}$) Digital Counts			
Module Temperature (°C)	-200	-250	-300
18	0.93	0.80	0.66
20	1.03	0.88	0.74
22	1.17	1.00	0.83
24	1.31	1.12	0.93

[a]Ardanuy, P., Nimbus-7 ERB PTM Coefficient Error Study, ERB Calibration Workshop Minutes, NASA Goddard Space Flight Center, pp. 25-35, 4-5 August 1982.

3. THE SORTING INTO ANGULAR BIN (SAB) ALGORITHM

The SAB method for processing the Nimbus-7 ERB scanner radiances assumes that during the averaging period a region (TA or latitude zone) is observed from many viewing directions such that the flux at the TOA can be evaluated by the following equation:

$$\overline{F} = \frac{\pi \int_o^{2\pi} \int_o^{\pi/2} \overline{M}(\theta, \phi) \cos\theta \sin\theta \, d\theta \, d\phi}{\int_o^{2\pi} \int_o^{\pi/2} \cos\theta \sin\theta \, d\theta \, d\phi} \quad , \tag{1}$$

where

θ	=	satellite zenith angle
ϕ	=	relative azimuth angle (0°, 180° plane contains the Sun in the 0° direction)
$\overline{M}(\theta,\phi)$	=	average observed radiance in an angular bin.

In terms of numerical integration, this becomes

$$\overline{F} = \pi W_k \overline{M_k} / \sum_{k-1}^{49} W_k \quad , \tag{2}$$

where

k	=	angular bin
W_k	=	angular weight; it is the integral of the denominator in (1) over just bin k.

When the angular sampling is incomplete, the weighted average is computed only over those bins which were sampled. Tests indicated that this procedure was about as accurate as trying to fill the empty bins by interpolation. In this algorithm, the chief problem concerns the adequacy of the data sampling. In our procedure, Earth radiation budget products are determined for two spatial domains, 4.5° latitude zones and (500 km)^2 target-area regions, and two temporal scales, daily and monthly averages. The sampling constraints of the ERB scanner prohibit the evaluation of regional fluxes on a daily basis. The typical number of angular bins sampled for the (500 km)^2 regions on a daily basis is around 15, inadequate to get a statistically meaningful flux. If the regions are sampled for a full month (generally 21-23 days because of restrictions in the ERB operating schedule), then the average number of angular bins sampled by the scanner generally ranges from 40 to 45, except near the poles. Figure 3-1 shows the mean number of angular bins for a region as a function of latitude for shortwave radiances during November 1979. The vertical arrows represent the standard deviation of the mean over all TAs in the latitude zone. In order to obtain Earth radiation budget products on a daily basis, it is necessary to increase the spatial domain over which the angular binning is performed. To accomplish this, we go to 4.5° latitude zones. When this is done, all angular bins are well sampled except bin numbers 44 to 46, which are typically undersampled or not viewed at all. The void in these bins

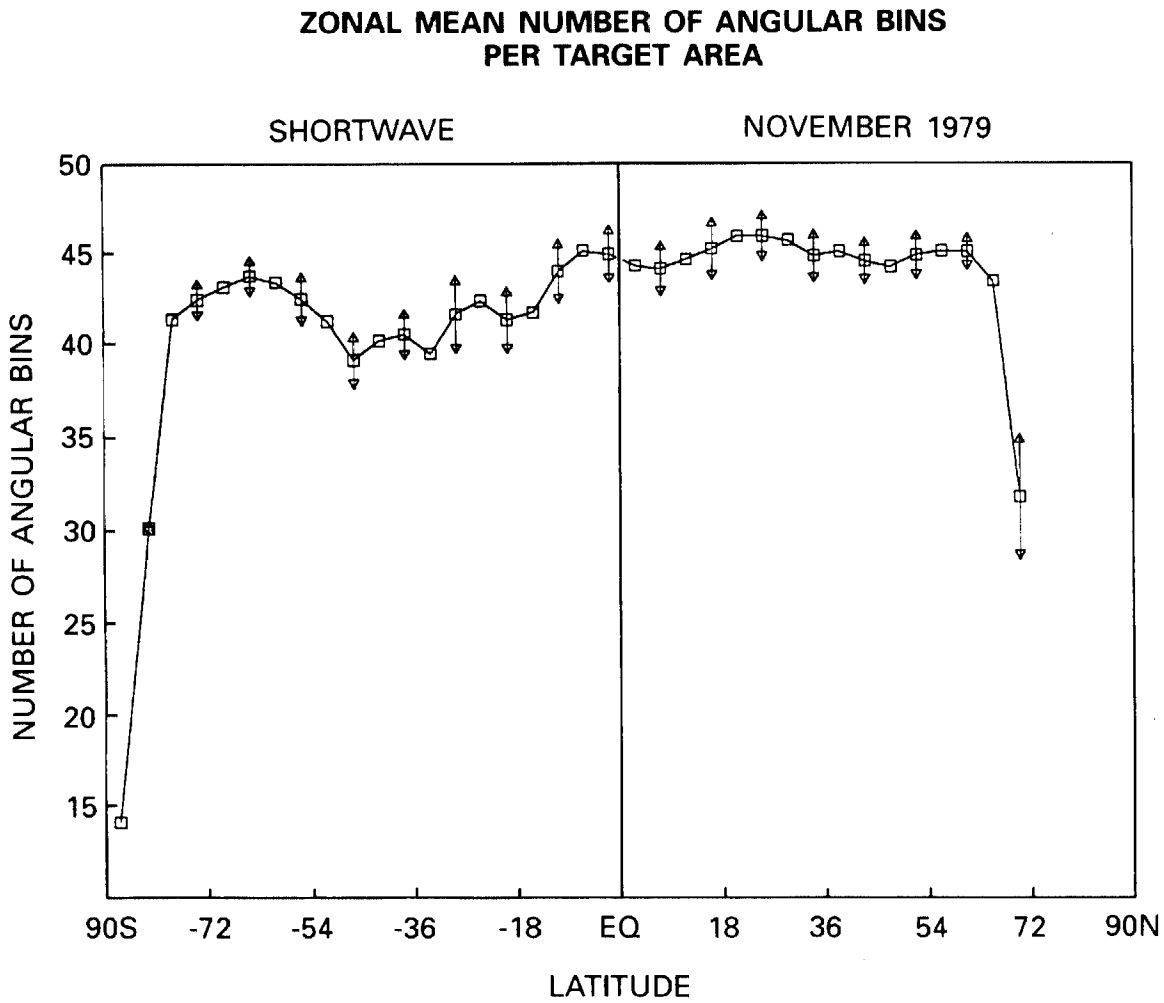

Figure 3-1. The mean number of angular bins sampled by the shortwave sensors, per TA, during the month of November. They are plotted as a function of latitude.

occurs because the satellite orbit plane is normally close to the principle (0-180° azimuth) plane in Figure 2-3. Thus, most of the data in bins 44-46 would be expected to come from the cross-track scans, but these stop at a satellite zenith angle of 71°. Figure 2-1 shows that regions near the subsatellite track are well sampled out to the horizon, but that there are significant angular gaps in the cross-track scanning. Sampling problems vary with latitude, season, and scanner operating mode. The satellite never passes beyond latitude 81°; thus, the polar zones are never sampled in enough bins to permit angular integration, while the neighboring zones (81° to 85.5° latitude) are marginally sampled on a zonal basis.

Table 3-1 shows the mean number of angular bins observed in individual TAs in representative latitude zones during November 1979. The average number of daily measurements in each bin is also shown. The daily populations are generally between 5 and 6. The average number of days that an angular bin is viewed depends on latitude and ranges from 6-9 days in the tropics and mid-latitudes to 10-22 days near the poles. The populations are averaged only over the days the bin is observed. Therefore, a typical angular bin near the equator is viewed 30 or 40 times during the month. The longwave sampling at night is similar but slightly smaller than the longwave daytime sampling. Also note the falloff in shortwave sampling starting near zone 36. This represents the decrease in sampling near the terminator, which is moving southward during November.

Table 3-1. Mean Number of Angular Bins Observed for a Target Area as a Function of Zone (for November 1979)

Zone	Latitude Bounds (°)	No. of TAs in Zone	Mean No. of Shortwave Bins	Daily Average Population[a]	Mean No. of Longwave-Day Bins	Daily Average Population
1	85.5-90.0S	3	14.0	41.0	15.0	55.8
2	81-85.5S	9	30.1	20.0	30.3	25.8
3	76.5-81.0	16	41.4	10.0	41.4	13.8
4	72.0-76.5	20	42.4	7.6	43.8	9.9
5	67.5-72.0	30	43.1	6.0	45.1	7.1
19	9.0-4.5S	80	44.9	5.4	45.5	5.8
20	4.5-0.0	80	44.7	5.4	45.3	5.8
21	0.0-4.5N	80	44.1	5.5	44.8	5.9
22	4.5-9.0	80	43.9	5.5	44.7	5.9
34	58.5-63.0	40	44.8	5.7	45.4	6.1
35	63.0-67.5	36	43.1	5.0	45.3	6.6
36	67.5-72.0	30	31.4	4.4	45.2	7.2
37	72.0-76.5	20	7.4	4.8	43.9	9.6
38	76.5-81.0	16	0.0	0.0	40.2	12.2
39	81.0-85.5	9	0.0	0.0	32.9	22.3
40	85.5-90.0N	3	0.0	0.0	15.7	50.3

[a]First the daily average in each bin is calculated counting only days in which the bin was observed. Then the mean for all observed bins in a target area is found. Finally, the mean for all observed target areas in the zone is calculated.

It was planned to do normal scanning in mode 5 (Figure 2-1) that gives maximum areal and angular coverage, and this was done for May 1979 through August 1979. However, mode 5 is actually a combination of modes 3 and 4 in which the side scan is done only to the right or to the left of the flight path, respectively. In early September, the automatic switching from mode 3 to mode 4 became defective. After that the scanner would operate in mode 3 for 3 days, be off one day and then operate in mode 4 for the next 3 days. This had only a small effect on the sampling in the equatorial regions. However, mode 3 sees just one of the poles, while mode 4 sees only the other. Thus, after early September, the polar zone and its nearest neighbor were viewed only half as often as previously. Since the SAB angular integration could not occur for the pole zones (1 and 40) at any time, the impact of this was moderate.

The accuracy of the numerical integration is normally only moderately affected by missing bins, except when their number becomes large. When only one bin is not sampled, it normally is one of the bins numbered 44-46 from the outer satellite zenith angle ring. However, when several bins are missing, they usually represent several satellite zenith angle rings. A test was made based on this fact. Zonal integrals with all bins sampled were tested for the effect of removing bins. Figures 3-2 and 3-3 show, for June 1979, the effect of removing bins from the albedo integral in a radial fashion starting with bin 45 and continuing until only the center bin remains. The order that the angular bins were omitted is as follows:

45, 37, 29, 21, 13, 5
48, 40, 32, 24, 16, 8
43, 35, 27, 19, 11, 3
47, 39, 31, 23, 15, 7
44, 36, 28, 20, 12, 4
46, 38, 30, 22, 14, 6
42, 34, 26, 18, 10, 2
49, 41, 33, 25, 17, 9

Several different zones from low to high latitudes are represented in the figure. In general, the northern hemisphere (Figure 3-2) appears to be fairly insensitive to missing data, except at high latitudes. In the southern hemisphere (Figure 3-3) we see that problems with missing data become somewhat more serious as the terminator is approached. The longwave test (not shown) indicates that the longwave integral varies only slightly when the first 18 or so bins are omitted entirely. The longwave test shows little difference between the northern and southern hemispheres.

This test shows that missing bins normally will not greatly affect the integral value, but it is, of course, not definitive. The data show strong limb darkening in the longwave; the shortwave have moderate limb brightening at 90° to the principle plane and strong limb brightening close to the principle plane. The shortwave integral becomes more sensitive at large solar zenith angles. Because of the poor sampling in bins 44-46, some of the longwave integrals may be slightly too large. The shortwave integrals, with 25% less data, will have their largest errors at high latitudes in the winter hemisphere.

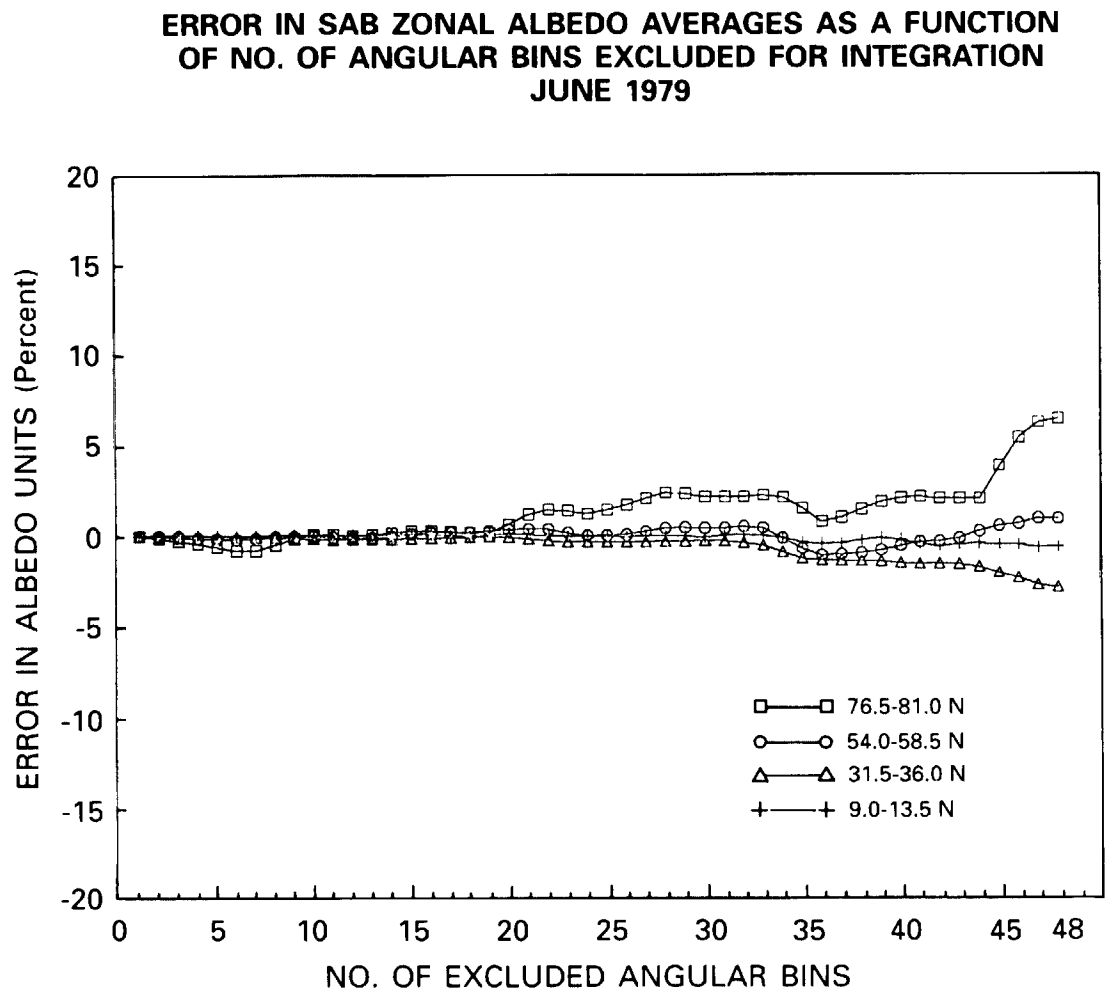

Figure 3-2. Effect of missing bins on the albedo integral. The resultant error is plotted against the number of excluded bins for several northern hemisphere zones in June 1979. See text.

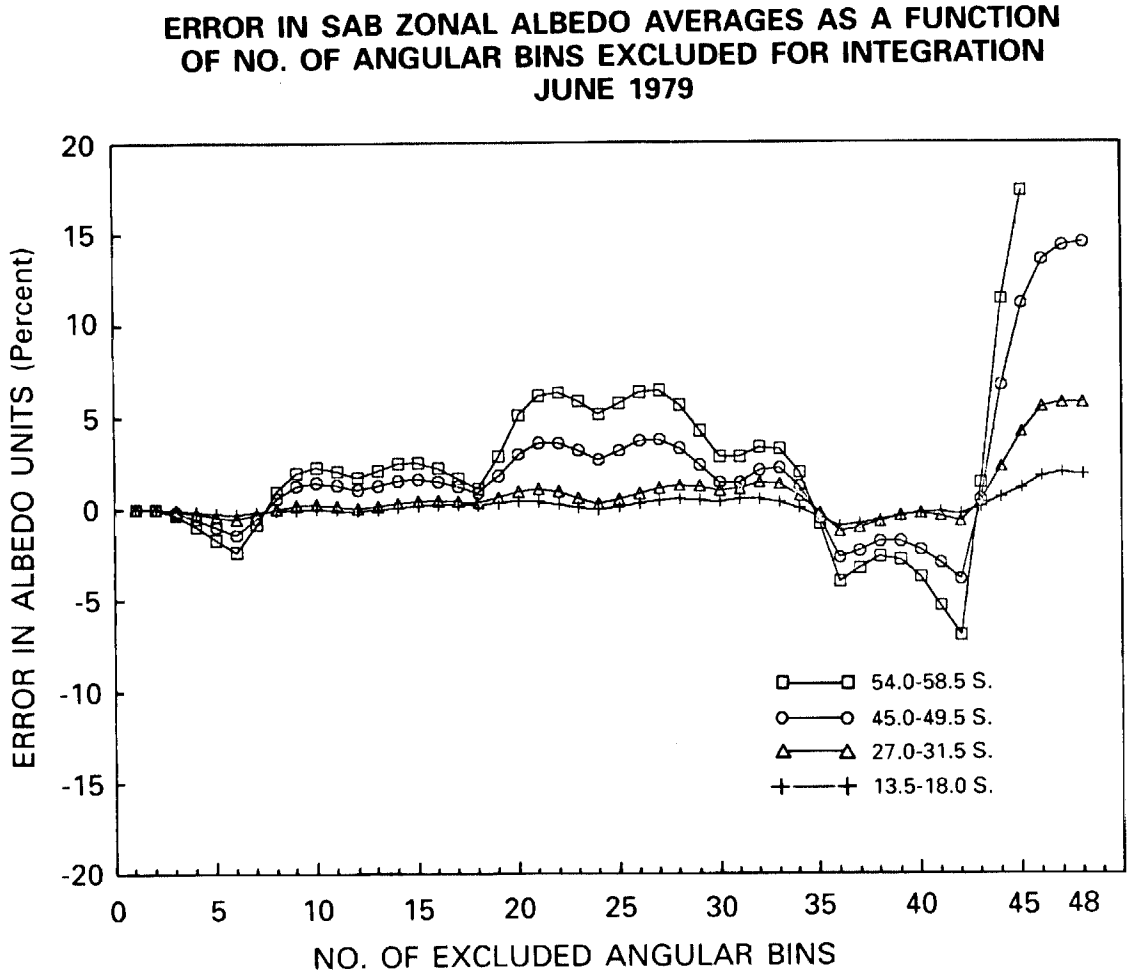

Figure 3-3. Similar to Figure 3-2, but here the zones are in the southern hemisphere, hence the solar zenith angle is larger. See text.

Because of the sampling problems, the TAs and zonal angular integrals will not give exactly the same results. Table 3-2 shows, however, that the methods give consistent results in terms of hemispherical and global averages. As should be expected, the shortwave with 25% less data shows somewhat poorer agreement than does the longwave.

Table 3-2. Annual Average Difference and Standard Deviation Between Target Area and Zonal-Daily Monthly Averages

	Northern Hemisphere	Southern Hemisphere	Global
Longwave (AN) (W/m^2)	-0.38 ± 0.3	-0.54 ± 0.4	-0.46 ± 0.3
Longwave (DN) (W/m^2)	-0.24 ± 0.5	-0.09 ± 0.4	-0.17 ± 0.3
Longwave (AVG) (W/m^2)	-0.18 ± 0.2	-0.15 ± 0.5	-0.16 ± 0.2
Shortwave (AN) (W/m^2)	+0.84 ± 1.2	+1.08 ± 0.8	+0.99 ± 0.7
Albedo (%)	+0.25 ± 0.2	+0.31 ± 0.2	+0.29 ± 0.1
Net Radiation (W/m^2)	+0.96 ± 0.6	+0.45 ± 0.8	+0.65 ± 0.5

*Difference expressed as regional-monthly minus zonal-daily.

On the SAB products tape, monthly mean albedo fields are provided for both 4.5° zone and TA spatial resolution. For each resolution, the time average over the month was performed as a simple arithmetic mean of daily albedo values for those days during which shortwave observations were taken. During the solstice months of June and December, when local solar insolation is changing only slowly during the month, this procedure is expected to give nearly the same result as the correct insolation-weighted albedo. Near the poles in early spring and fall, however, daily values of solar insolation are changing relatively rapidly and the arithmetic average might yield an incorrect result. This would occur if, for example, an albedo trend existed during the month. We investigated this possibility for the months of June 1979 and April 1980. Results for April are shown in Figure 3-4, where the monthly mean daily albedos for zonal resolution are shown as a function of latitude. The solid curve is the unweighted albedo appearing on tape, while the dotted curve gives the correction required to obtain the insolation-weighted albedo. The albedo correction is negligible for most latitude bands (±0.2%) but, as expected near the South Pole for latitudes between -70° and -80°, a negative correction of on the order of 1% (albedo units) is found. The sign of this correction corresponds to an increase in daily albedo as the solar illumination decreases during the month. Near the North Pole, a slight albedo increase (0.3%) is indicated by the correction curve. This result does not conform to the usual trend of decreasing albedo with increasing solar declination as the Sun moves into the northern hemisphere at this time of year. The positive value is probably an indication of the limit in accuracy of the SAB method within the three latitude bands nearest each pole. Depending on the ERB operating schedule and the scanner sampling mode (see Section 2 and Table 2-2), these bands are viewed infrequently (perhaps as infrequently as 5-day intervals), and a noisy monthly mean is likely to occur. For June, the insolation-weighted monthly albedo was found to be the same as the SAB albedo to within 0.2% for all latitudes.

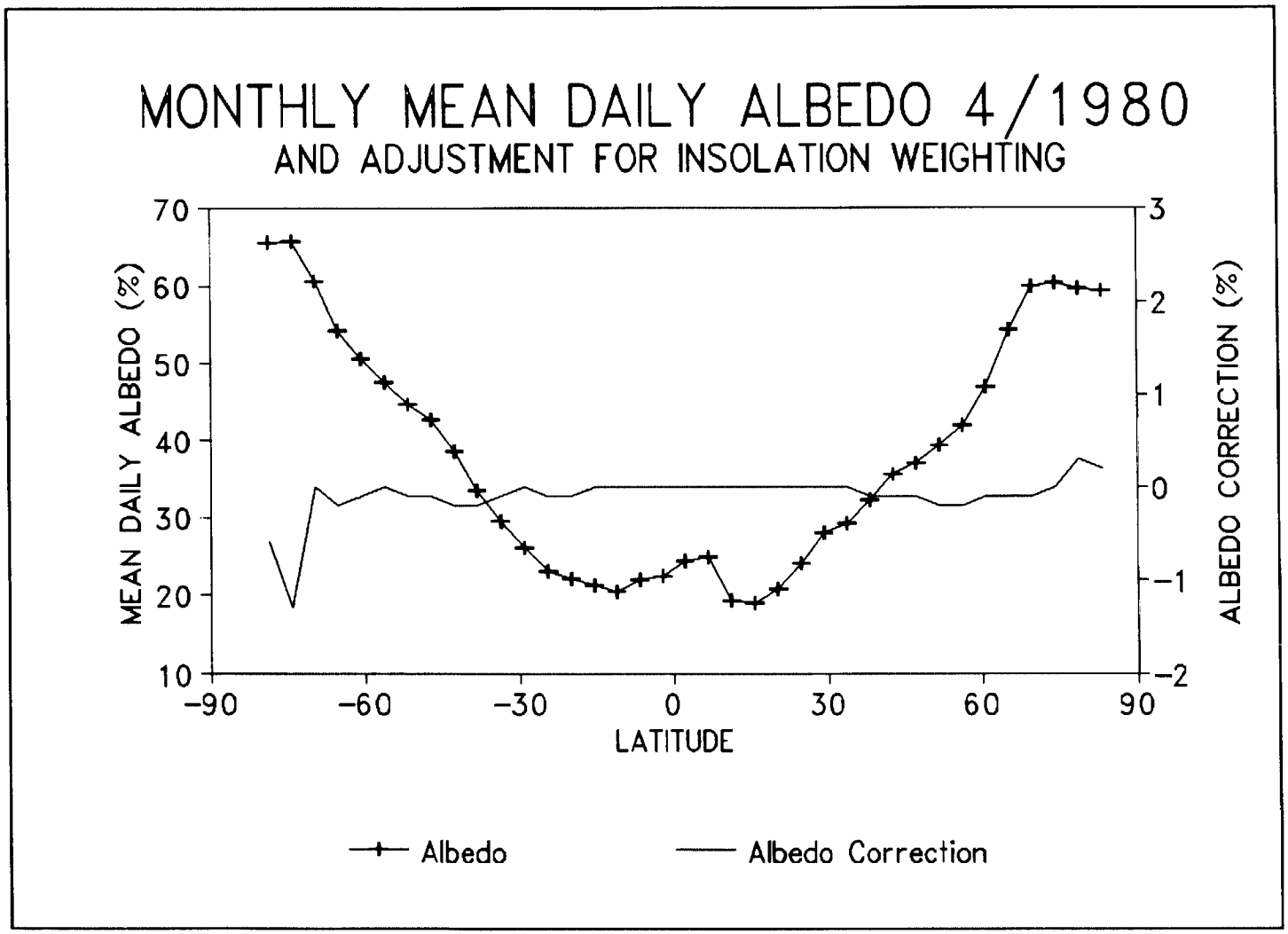

Figure 3-4. The calculated SAB monthly mean albedos were arithmetic means of the daily values. The daily values should have been weighted by the daily insolation when forming the monthly mean. The small corrections for the zonal averages are shown here.

4. MAXIMUM LIKELIHOOD CLOUD ESTIMATION ALGORITHM

This is a statistical procedure for converting an NFOV radiance measurement, M, into a flux estimate, F. If the radiance field is isotropic, the conversion is simply

$$F = \pi M \quad . \tag{3}$$

However, many Earth scenes are highly anisotropic, and a more accurate procedure is required. The MLCE procedure we use is based on a similar ERBE algorithm, which has been described in detail by Wielicki and Green (1989). We will, therefore, give a brief description here, and we will mention some of the differences between the two algorithms. The MLCE method assumes that the various Earth/atmosphere radiance fields can be adequately described by 12 bidirectional models, derived principly from the Nimbus-7 ERB scanner data (Suttles et al., 1988). There are five surface types: ocean, land, desert, coast, and snow. These are designated by a map. There is only one overcast scene (95% to 100% cloud cover), but three partly cloudy (5% to 50% cloud cover) and three mostly cloudy (50% to 95% cloud cover) scenes. There are separate partly cloudy and mostly cloudy scenes for ocean, coasts, and land/desert.

The shortwave scenes are global in extent and are dependent on satellite zenith and azimuth angle, as well as the solar zenith angle. The longwave limb darkening models depend on season (spring, summer, fall, and winter), latitude and satellite zenith angle, but not on solar zenith angle or satellite azimuth angle (Suttles et al., 1989).

After the surface type is determined from a map, the correct cloud scene (clear, partly cloudy, mostly cloudy, or overcast) is determined by checking the observed shortwave and longwave radiance pair against the appropriate models. A Maximum Likelihood Estimation (MLE) algorithm is used.

The probability that a particular cloud cover produces the scanner shortwave radiance measurement, M_{SW}, and longwave radiance measurement, M_{LW}, is given by

$$P_c = \frac{1}{[2\pi\sigma_c(SW)\ \sigma_c(LW)\ (1 - r_c^2)]^{1/2}}\ e^{-G/2} \tag{4}$$

where

$$G = \frac{1}{(1-r_c^2)} \left\{ \left[\frac{M_{SW} - L_c(SW)}{\sigma_c(SW)} \right]^2 - 2r_c \left[\frac{(M_{SW} - L_c(SW))\ (M_{LW} - L_c(LW))}{\sigma_c(SW)\ \sigma_c(LW)} \right] + \left[\frac{M_{LW} - L_c(LW)}{\sigma_c(LW)} \right]^2 \right\} \tag{5}$$

c	=	cloud/geography type
M_{LW}	=	longwave radiance measurement
M_{SW}	=	shortwave radiance measurement
$L_c(LW)$	=	model longwave radiance
$L_c(SW)$	=	model shortwave radiance
$\sigma_c(SW)$	=	standard deviation of the elements of a shortwave bidirectional model
$\sigma_c(LW)$	=	standard deviation of the elements of a longwave anisotropic model
r_c	=	correlation coefficient between shortwave and longwave radiances for each angular bin of the shortwave model.

The cloud scene with the largest probability is chosen and the desired fluxes calculated as follows:

$$F_{LW} = \pi M_{LW}/R_c(LW) \tag{6}$$

$$F_{sw} = \pi M_{SW}/R_c(SW) \tag{7}$$

$R_c(LW)$	=	model scene longwave limb darkening function
$R_c(SW)$	=	model scene shortwave angular dependence model (ADM).

If only one radiance (longwave or shortwave) was measured, then it was used by itself to identify the cloud scene. In this case, the missing radiance and the correlation coefficient were dropped from Eqs. (4) and (5). At night, of course, only the longwave radiances are present. In practice, for simplicity, the correlation term was set equal to zero all the time in both algorithms. This had little effect on the mean results. Additional tuning and adjustment of the models was required in order to get the best results. This tuning differed somewhat between the Nimbus ERB and the ERBE cases so that the end algorithms are not identical.

If the models and scene identification procedure worked perfectly, then the calculated longwave and shortwave fluxes from a given scene could be independent of the satellite zenith angle. In practice, however, at large satellite zenith angles, the calculated longwave flux values were too small and the shortwave fluxes too large. This is shown in Figures 4-1 and 4-2. For June 1979, the ascending node longwave fluxes and observed albedos from 60°S to 60°N latitude were collected by satellite zenith angle and plotted. When the satellite was near the zenith, the average OLR was 254 W/m^2, but this dropped to 235 W/m^2 when the satellite was near the horizon. In the shortwave case, the average albedo was 23.9% when observed near the zenith, but rose to 26.3% when observed near the horizon. Comparison with both the Nimbus SAB results and the WFOV measurements indicated that the MLCE algorithm yielded incorrect results from measurements made at large satellite zenith angles. This is a fairly serious problem in the Nimbus ERB case, because the scanner is designed to take considerably more measurements at large zenith angles than at small ones. It was decided to reject all measurements made at satellite zenith angles greater than 75°. This produced reasonable agreement with both the SAB and WFOV measurements (see Table 5-2), but the MLCE albedos may be about 1% too large. The ERBE scanner has a fixed aperature whose footprint becomes quite large near the horizon. For this and other reasons, the ERBE algorithm, from the beginning, rejected all satellite zenith angles larger than 70°. When Brooks and Fenn (1988a,b) changed the ERBE algorithm to accept satellite zenith angles greater than 70°, they obtained results similar to ours.

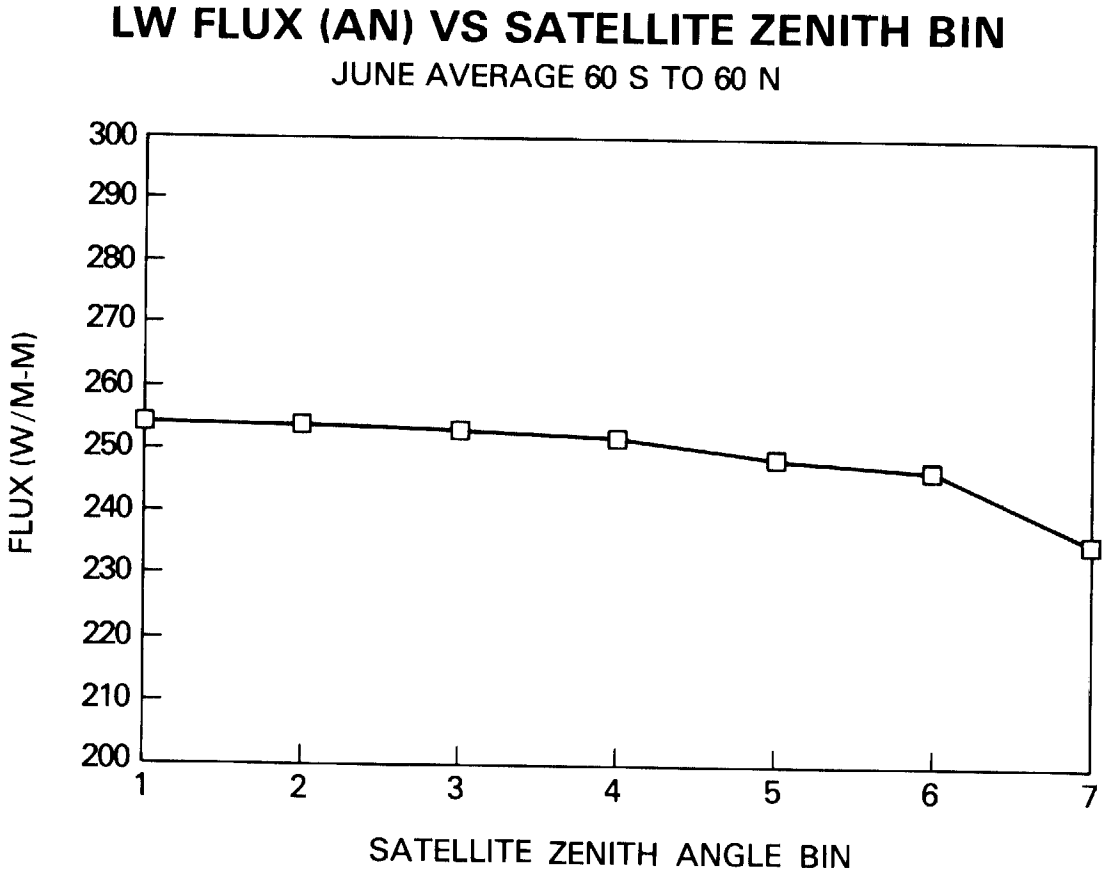

Figure 4-1. Longwave (LW) fluxes estimated by MLCE procedure as a function of satellite zenith angle. The zenith angle bins are numbered from nadir with boundaries at 15°, 27°, 39°, 51°, 63°, and 75°. See Figure 2-3.

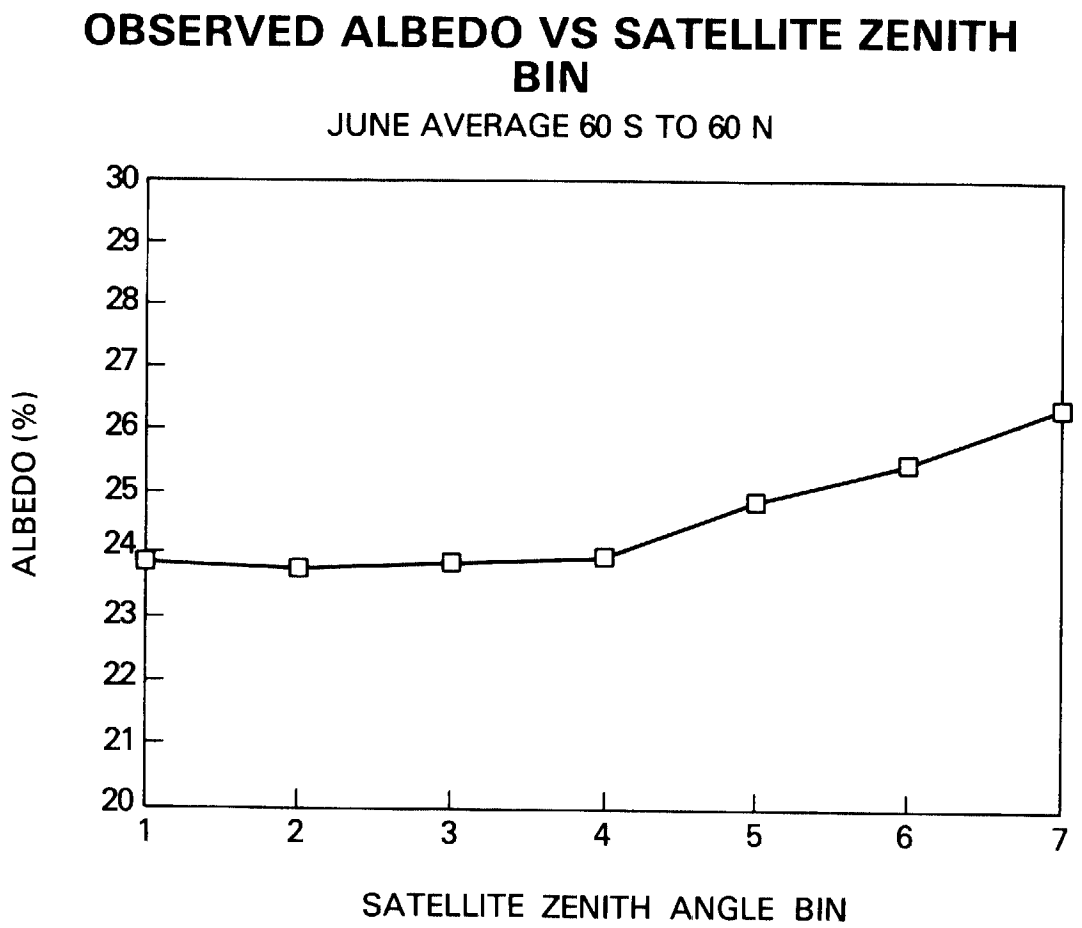

Figure 4-2. MLCE estimated albedos as a function of satellite zenith angle. The zenith angle bins are numbered from nadir. See Figure 4-1.

These MLCE algorithm problems at large satellite zenith angles may be partially because of deficiencies in the models, but, at least in the shortwave case, much of it comes from ambiguities in scene identification, particularly over the ocean. Near the horizon, measured radiances from clear and overcast ocean scenes may be at times nearly identical, but the integrated shortwave fluxes might differ by a factor of two or more. The model radiance standard deviations used in Eqs. (4) and (5) are considerably larger for overcast scenes than for clear scenes. Thus, in such a case, the algorithm will usually decide that the scene is more probably overcast (or mostly or partly cloudy) than clear. The problem is compounded by the fact that because of geometric considerations, the observed cloud amount is normally larger at the horizon than at the nadir. This is illustrated in Figure 4-3. In Figure 4-4, the scene identification is shown as a function of satellite zenith. Averages are shown for June 1979 for measurements taken between 60°S and 60°N latitude. Brooks and Fenn (1988a,b) obtained similar results from the ERBE algorithm using ERBE scanner measurements and accepting satellite zenith angles past 70°.

The ERBE team did some additional tuning of their algorithm, and these additions are not present in the Nimbus ERB algorithm. Considerable interest in the clear-sky radiances has developed (Ramanathan et al., 1989a,b; Ardanuy et al., 1989), and most of these additions aim at improving the clear-sky products. In determining cloud-scene probabilities, the ERBE team multiplies the MLE probabilities (Eq. 4) by a priori climatological cloud-scene probabilities derived from the Nimbus-7 cloud data set (see Wielicki and Green, 1989). The different model cloud-scene probabilities have large overlap regions, and this procedure was used to push the choices in the climatologically correct direction. For instance, it increases the amount of clear desert regions identified. When we applied these a priori factors to the Nimbus-7 ERB data, however, we found that the number of clear ocean regions became extremely small in many regions, including some where few clouds were known to be present. In particular, no clear-sky regions were found at night over very large ocean regions. Because of this, we did not use the a priori cloud-statistic factors. It should be emphasized that the use of the a priori cloud factors seems to have very little effect on the all-sky fluxes determined by the MLCE algorithm, even though they do readjust the various component cloud-scene fluxes; this is true in both the Nimbus-7 ERB and the ERBE products.

Finally, it should be noted that in the Nimbus-7 ERB algorithm, we used just the 12 sets of solar zenith angle dependent model scene albedos presented in Suttles et al. (1988). However, over land and desert, the ERBE team introduced many subcategories dependent on vegetation cover desert albedo characteristics. This undoubtedly improved their clear-sky identifications over land and desert.

The MLCE radiance to flux conversion algorithm is a great improvement over older such procedures such as the isotropy approximation (Eq. 3) or the original Nimbus-7 ERB algorithm (Jacobowitz et al., 1984a). However, it is also much more complicated and must be applied with care and tuned to the data set being processed.

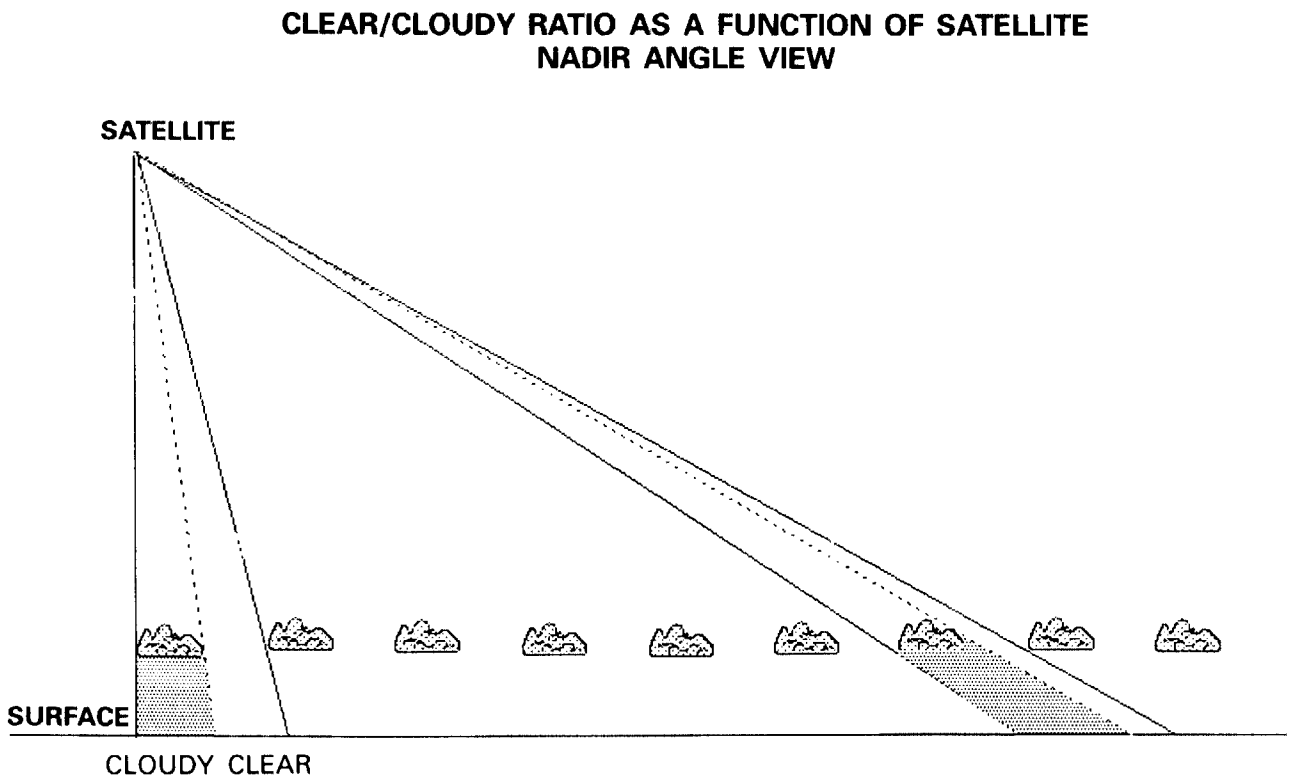

Figure 4-3. Effect of the satellite zenith angle on the observed clear/cloudy ratio.

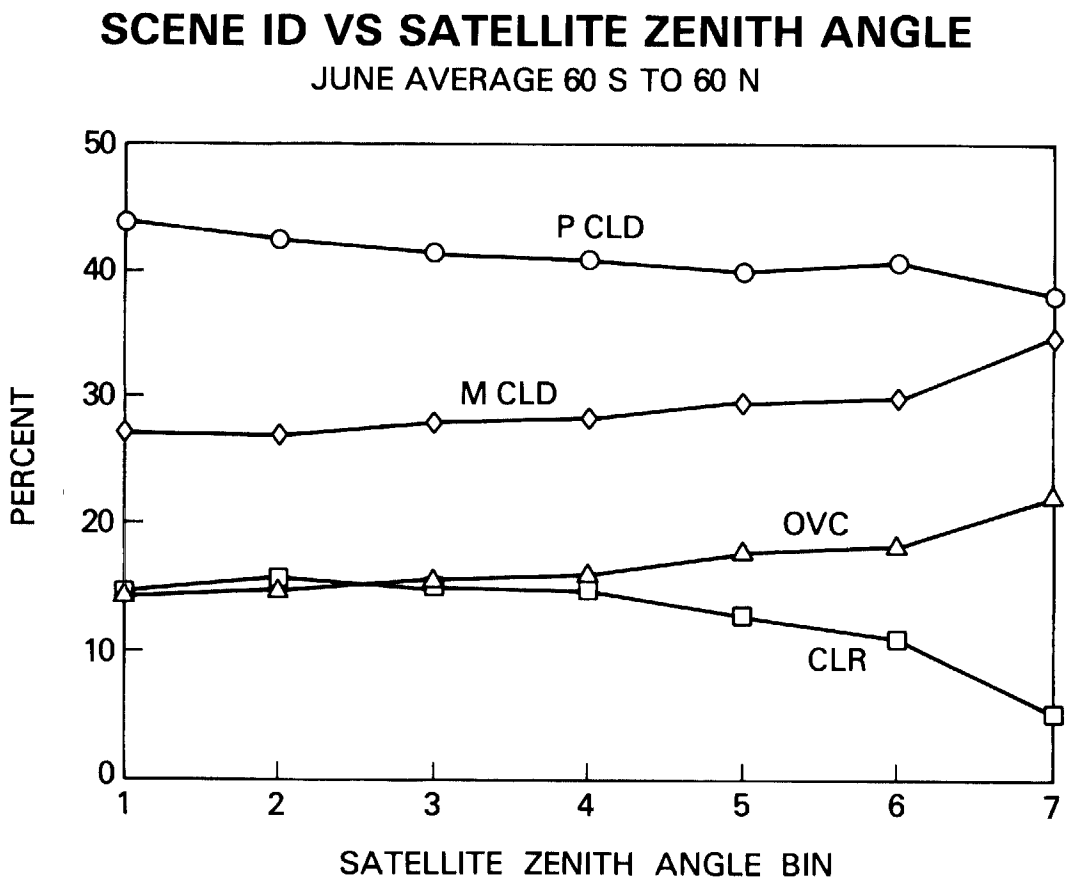

Figure 4-4. Percent of cloud scene type identified as a function of satellite zenith angle. The four MLCE cloud scenes are: clear, partly cloudy, mostly cloudy, and overcast.

5. DIURNAL CORRECTION MODELS

The Nimbus-7 satellite is in a Sun-synchronous orbit and observes most of the Earth twice a day, once near noon and once near midnight local time. Some assumptions, therefore, must be made in order to estimate the average diurnal OLR and albedo. For the OLR, it is assumed that the mean of the noon and midnight measurements also represents the diurnal mean. A study by Kyle et al. (1990) found this to be statistically a very good approximation over the ocean in the mean, but that it was 1% or 2% too high over land. Over deserts in the summer this approximation is 2% too large.

Diurnal models of how the albedo varies with solar zenith angle are used to estimate the daily averaged albedo from a once-a-day observation. Different sets of diurnal models were used in the SAB, MLCE, and WFOV global Calibration Adjustment Table (CAT) production programs. This is due partially to differences in the measurements and the way they are treated in the algorithms, but historical development is the chief reason. In 1979 the Nimbus-7 ERB team picked diurnal models to use in the NFOV and WFOV processing. For the NFOV they chose three scene-dependent models (ocean, land/cloud, and snow) based on the work of Raschke et al. (1973). They also formed a scene-independent (90% cloud/land +10% ocean) model from these for use with the WFOV measurements (Kyle et al., 1986). When the new global CAT algorithm was adopted in 1985, it was decided to keep the original WFOV diurnal albedo model. In 1986, when the NFOV algorithm SAB and the WFOV-enhanced resolution algorithms were being developed, the new ERBE models became available (Brooks et al., 1986). For this work, five of the ERBE models (ocean, land, desert, snow, and overcast) were chosen, together with time-averaged cloud fields from the Nimbus-7 cloud data set (Stowe et al., 1988, 1989). The models used are shown in Table 5-1. Our MLCE algorithm is based directly on the ERBE procedure so it, of course, uses all 12 of the ERBE albedo diurnal models. The partly cloudy and mostly cloudy ERBE models lie between the clear and cloud models shown in Table 5-1, but they are not a linear function of the clear and cloud models and the cloud fraction. Parenthetically, it should be noted that, while we used the models described in Brooks et al. (1986) and Suttles et al. (1988), the ERBE team has since introduced modified clear desert and mostly cloudy over land/desert models. Thus, differences in diurnal models combine with differences in the calculation of the observed albedos to produce differences in the Earth radiation budget products.

Monthly globally averaged OLR and albedo from both the old and new NFOV Nimbus-7 ERB algorithms are listed in Table 5-2 for July 1979 and January 1980, together with the corresponding WFOV values. In addition, both Nimbus-7 WFOV and ERBE scanner averages for July 1985 and January 1986 are shown for comparison. In the old NFOV algorithm, observed albedos were not listed, but the diurnally corrected values were nearly 10% larger than the WFOV values. The new SAB observed albedos vary from 0.4% smaller in July to 1.8% larger in January than the observed global CAT albedos. As expected, our MLCE calculations of the observed albedos are somewhat larger (2%) than the SAB values. However, the mean SAB diurnal correction factor is about 2.5% smaller than that for the global CAT, while the mean MLCE factor (1.12) is the same as that for the global CAT. Thus, the diurnally averaged SAB albedos are smaller and the MLCE albedos larger than the global CAT values. Finally, global CAT and the new ERBE scanner albedos are compared for July 1985 and January 1986. The two values are identical in July, while the ERBE value is about 1% larger in January.

Table 5-1. ERBE and Nimbus-3 Directional Reflectance Models						
Range of cos (ζ_{sun})	Ocean	Land	Snow	Desert	Cloud	Nimbus-3
1.0 - 0.9	1.00	1.00	1.00	1.00	1.00	1.00
0.9 - 0.9	1.08	0.98	1.00	1.01	1.02	1.00
0.8 - 0.7	1.20	1.02	1.01	1.02	1.07	1.09
0.7 - 0.6	1.33	1.04	1.01	1.03	1.13	1.18
0.6 - 0.5	1.51	1.09	1.02	1.04	1.18	1.30
0.5 - 0.4	1.75	1.16	1.02	1.06	1.25	1.41
0.4 - 0.3	2.12	1.28	1.02	1.09	1.32	1.56
0.3 - 0.2	2.67	1.44	1.01	1.13	1.39	1.68
0.2 - 0.1	3.53	1.69	0.97	1.21	1.46	1.78
0.1 - 0.0	4.40	2.04	0.93	1.31	1.52	1.84
The Nimbus-3 model was obtained from Table 2 of Hucek et al. (1987). The ERBE models come from Brooks et al. (1986).						

As a test, the WFOV scene-independent diurnal model was applied to the SAB data for the months of July 1979 and January and April 1980. The global mean results are shown in Table 5-3 as differences between the ERBE and WFOV directional model results. The WFOV directional model produces mean diurnal albedos just a little larger than the MLE albedos. Recall, however, that only five of the ERBE models (see Table 5-1) are used in the SAB processing. As mentioned above, the use of all 12 models in Nimbus ERB MLE processing produced a mean diurnal correction similar to the WFOV model value. The use of a scene-independent diurnal model introduces regional errors even if the global mean is correct. Regional SAB albedos computed using both the scene-dependent and scene-independent models are compared in Table 5-4. In the mean, the scene-independent correction factor is larger (see Table 5-3), but for clear ocean scenes, the scene-dependent model yields larger albedos. Also note the large differences in the clear desert and snow cases.

Our conclusion is that the observed MLCE albedos are slightly too large, but that the MLCE diurnal correction factors are, in the mean, slightly better than the SAB factors. This would indicate that cloud diurnal correction models should vary with cloud amount and probably with cloud type. However, since both cloud amounts and types often vary during the day, there is a limit to how accurately regional diurnal albedo averages can be estimated from once-a-day observations. The ERBE data set has an advantage here, because the ERBS satellite observes regions between 57°S and 57°N latitude at least once during every hour of the day in 37-day cycles.

The OLR derived from the global CAT, SAB, and MLCE algorithms normally agree to better than 1%. The largest difference shown in Table 5-2 is for July 1979, where the SAB ascending node value is 1.1% higher than the global CAT value. Note that the global CAT and ERBE scanner averages agree to 0.5% or better in July 1985 and January 1986. Overall, the new Nimbus-7 ERB products show a good internal agreement, as well as a quite reasonable agreement with the independent ERBE data set. Some regional values, of course, show larger variations than indicated in Table 5-2. In addition, the WFOV sensors smooth the regional values so that regional WFOV and NFOV products are not directly comparable (see Kyle et al.,

1990). The biggest uncertainty lies in the models used to convert observed to daily averaged albedos. Here the Nimbus WFOV products suffer regionally, because a scene-independent model is used. The SAB single-cloud model also appears inferior to the multiple-cloud models used by the MLCE algorithm. The global CAT, SAB, and MLCE products are all of good quality and can be recommended for most climate studies.

Table 5-2. Comparison of Nimbus-7 Earth Radiation Budget Products: Global Averages

	OLD NFOV			NEW WFOV			NEW NFOV						ERBE/NFOV
				GLOBAL CAT			SAB			MLE			ERBS/NOAA 9
OLR (W/m^2)													
Month	AN	DN	AVG	AN	DN	AVG	AN	DN	AVG	AN	DN	AVG	AVG
JUL 79	239.4	234.3	237.1	241.4	237.1	239.3	244.1	237.3	240.7	243.0	236.8	239.9	
JUL 85				240.5	235.3	237.9							237.5
JAN 80	232.7	227.7	230.2	237.2	231.5	234.4	237.2	231.5	234.3	235.5	230.6	233.1	
JAN 86				235.8	230.7	233.2							231.9
ALBEDO (%)													
	D. AVG			OBS	D. AVG		OBS	D. AVG		OBS	D. AVG		D. AVG
JUL 79	32.7			26.4	29.6		26.3	28.8		26.8	30.1		
JUL 85				26.0	29.2								29.2
JAN 80	33.6			26.9	30.1		27.4	29.9		28.0	31.3		
JAN 86				27.2	30.5								30.9

Table 5-3. Comparison of Hemispheric/Global Averages of Daily Averaged Albedo and Net Radiation Using ERBE and WFOV Directional Models

	July 1979	January 1980	April 1980
DAILY AVERAGED ALBEDO (%)			
Northern Hemisphere	-1.3	-0.8	-1.3
Souther Hemisphere	-0.5	-1.3	-0.7
Global	-1.1	-1.1	-1.1
NET RADIATION (W/m^2)*			
Northern Hemisphere	+5.9	+1.8	+5.3
Southern Hemisphere	+1.1	+6.1	+2.0
Global	+3.5	+4.0	+3.7

*Difference between monthly averaged values expressed as ERBE model minus WFOV model based on Nimbus-7 ERB scanner observations processed using a direct SAB method of integration.

Table 5-4. Comparison of Regional Daily Averaged Albedo Using Scene-Dependent SAB (ERBE) and Scene-Independent (WFOV) Diurnal Models for July 1979

Region	SD-ERBE	SI-WFOV	Δ Models (%)	Cos ζ_{sun}
Clear Land (Northern Australia)	20.6	21.7	-1.1	0.79
Clear Land (South Central Africa)	16.1	17.0	-0.9	0.84
Clear Desert (Sahara)	31.5	34.9	-3.4	0.99
Clear Ocean (Southeastern Pacific Ocean)	12.7	12.2	+0.5	0.88
Clear Ocean (Southeastern Pacific Ocean)	11.8	11.0	+0.8	0.91
Clear Snow (Arctic Ocean)	48.4	52.1	-3.7	0.51
Overcast (India)	36.6	38.5	-1.9	0.99
Overcast (Bay of Bengal)	35.9	37.7	-1.8	0.98

6. THE EARTH'S RADIATION BUDGET, 1979/80

The Sun is the original energy source for both life on Earth and the Earth's climate system. TOA net radiation maps show where the solar energy is principly absorbed. Figures 6-1 to 6-4 are, respectively, the net radiation maps for July and October 1979 and January and April 1980. The dashed contours indicate negative values where more energy is lost than is received.

In July (Figure 6-1), the subsolar point is a little south of the Tropic of Cancer, while the maximum heating occurs in the ocean slightly north of this line. The land areas are normally less efficient than the oceans in absorbing solar energy, and this is particularly true of the deserts. Note the negative net radiation in the east central Sahara. Also note the local minima in the net radiation off the west coasts of California, South America, and southern Africa. These are associated with persistent fields of low stratus clouds that block the incident solar flux. Their relatively low, warm cloud tops allow efficient escape of the thermal infrared.

Figures 6-2 (October) and 6-3 (January), show how the net radiation maxima move southward, tracking the subsolar point. In January, with the Sun at perihelion, a broad maximum covers much of the southern ocean on either side of the Tropic of Capricorn. It bulges more to the south than to the north, however. As in the north, the southern land masses are relatively poor absorbers of net radiation. By April, Figure 6-4, the net radiation maxima have moved back north of the Equator.

Examples of the OLR and albedo fields are shown, respectively, in Figures 6-5 and 6-6 for July 1979. There is a strong anticorrelation between the OLR and albedo fields. The OLR high of 298 W/m^2 in the Pacific west of Peru is associated with an albedo low. Most albedo and OLR maxima and minima over the ocean are similarly linked at low- and mid-latitudes. In contrast, both the OLR and albedo are high over the Sahara, where both are chiefly dependent on the surface conditions rather than on the cloud fields. This explains the low net radiation there.

Comparing the OLR and albedo maps with the net radiation (Figure 6-1) shows distinctly different patterns. However, the local net radiation maxima tend to associate with low albedo values. But note that there is not a strong correlation of the longwave maxima with the net radiation maxima.

Further analysis of the Earth's radiation budget, using Nimbus-7 data, can be found in Hartmann et al. (1986), Jacobowitz et al. (1984b), Kyle et al. (1986), Ramanathan (1987), and Smith and Smith (1987).

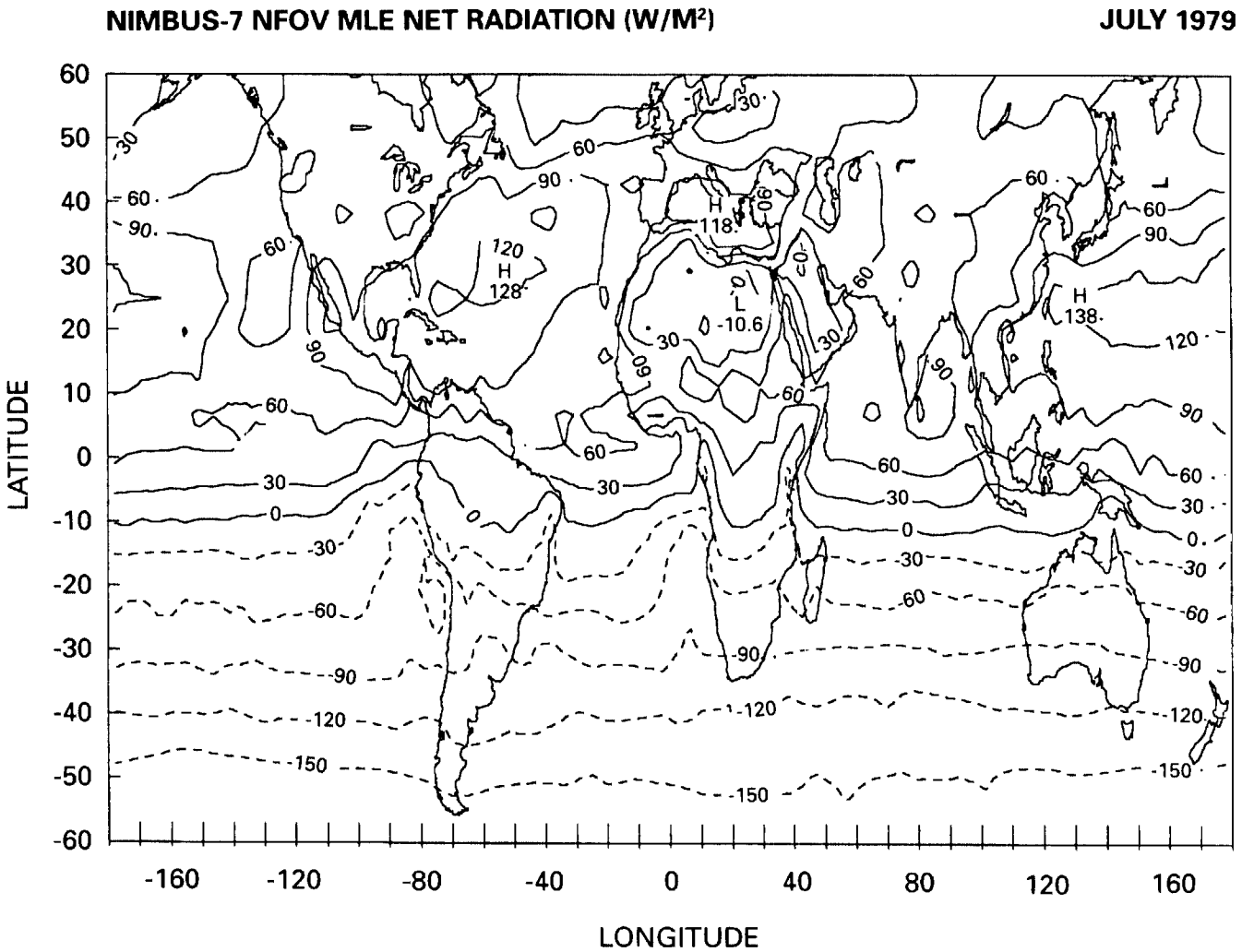

Figure 6-1. Map of monthly averaged net radiation for July 1979 calculated by the MLCE procedure.

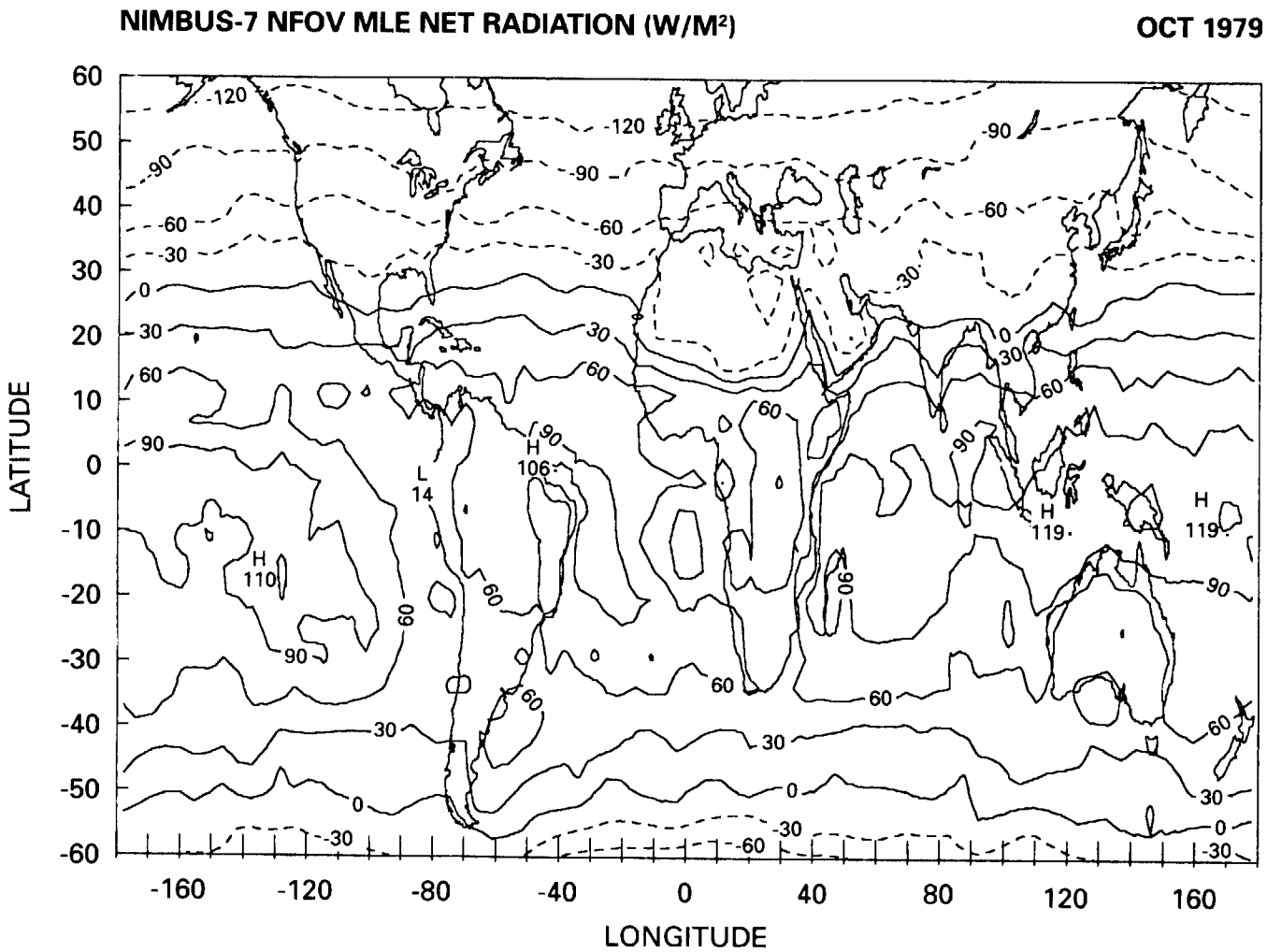

Figure 6-2. Map of net radiation for October 1979; MLCE algorithm results.

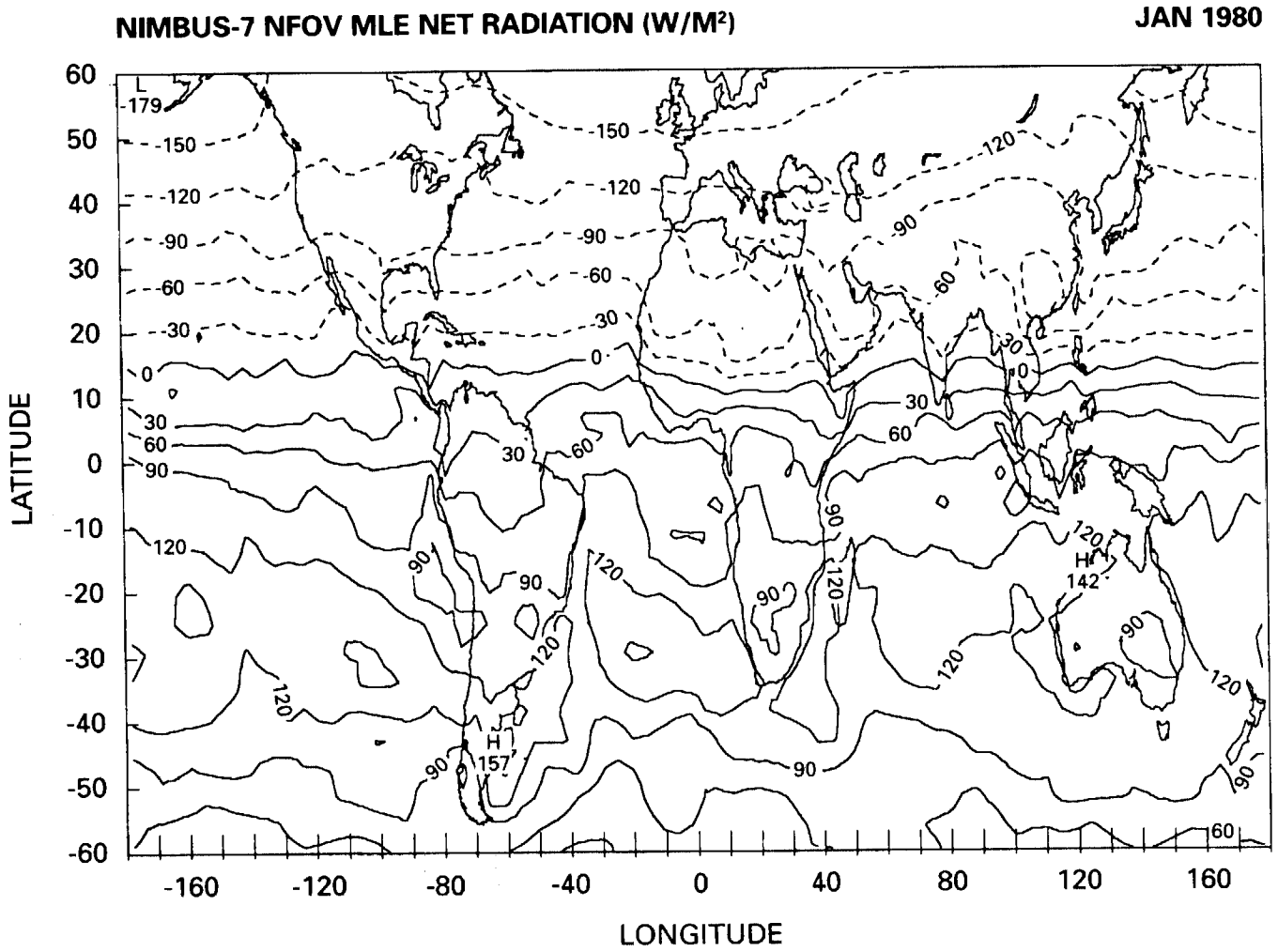

Figure 6-3. Map of net radiation for January 1980; MLCE algorithm results.

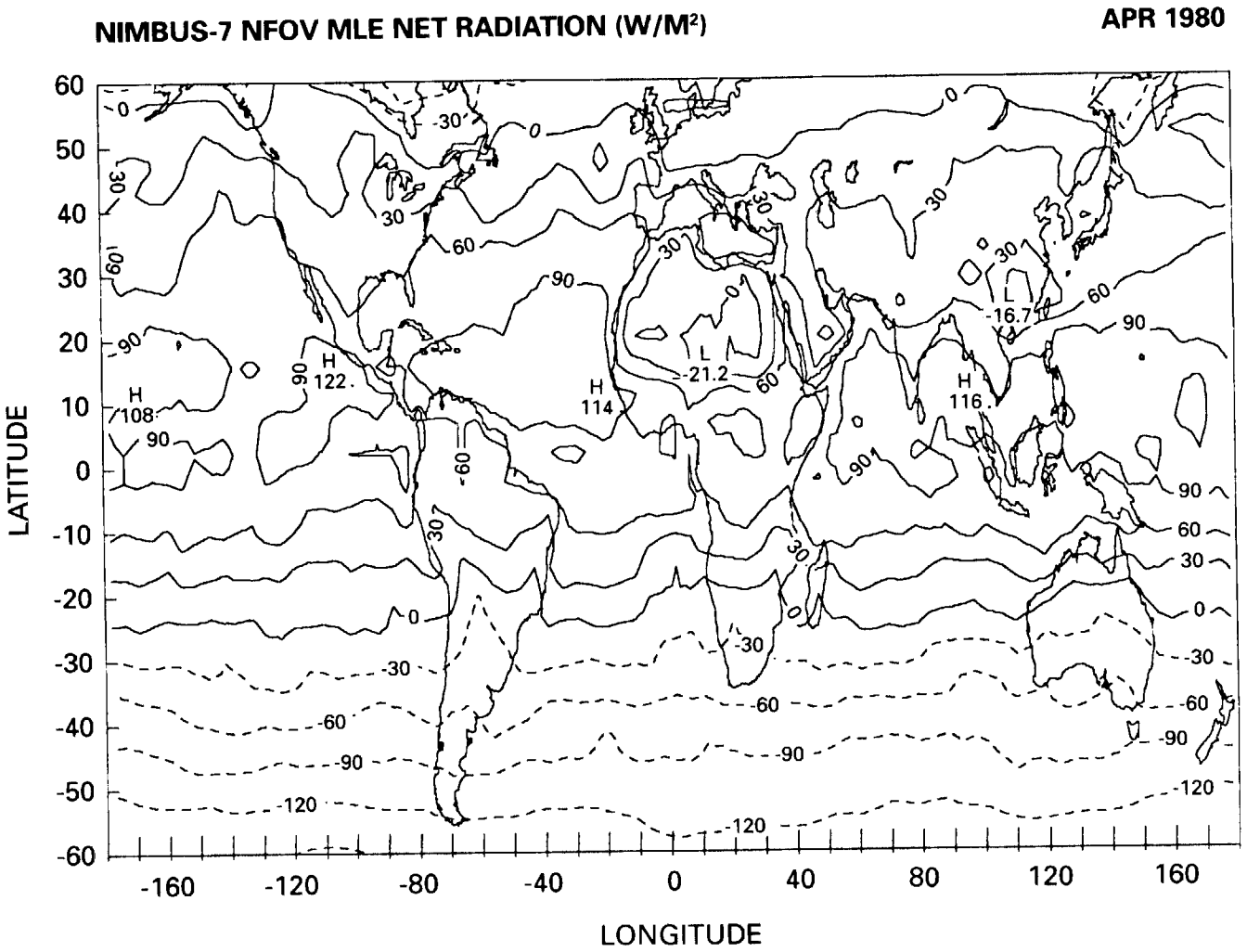

Figure 6-4. Map of net radiation for April 1980; MLCE algorithm results.

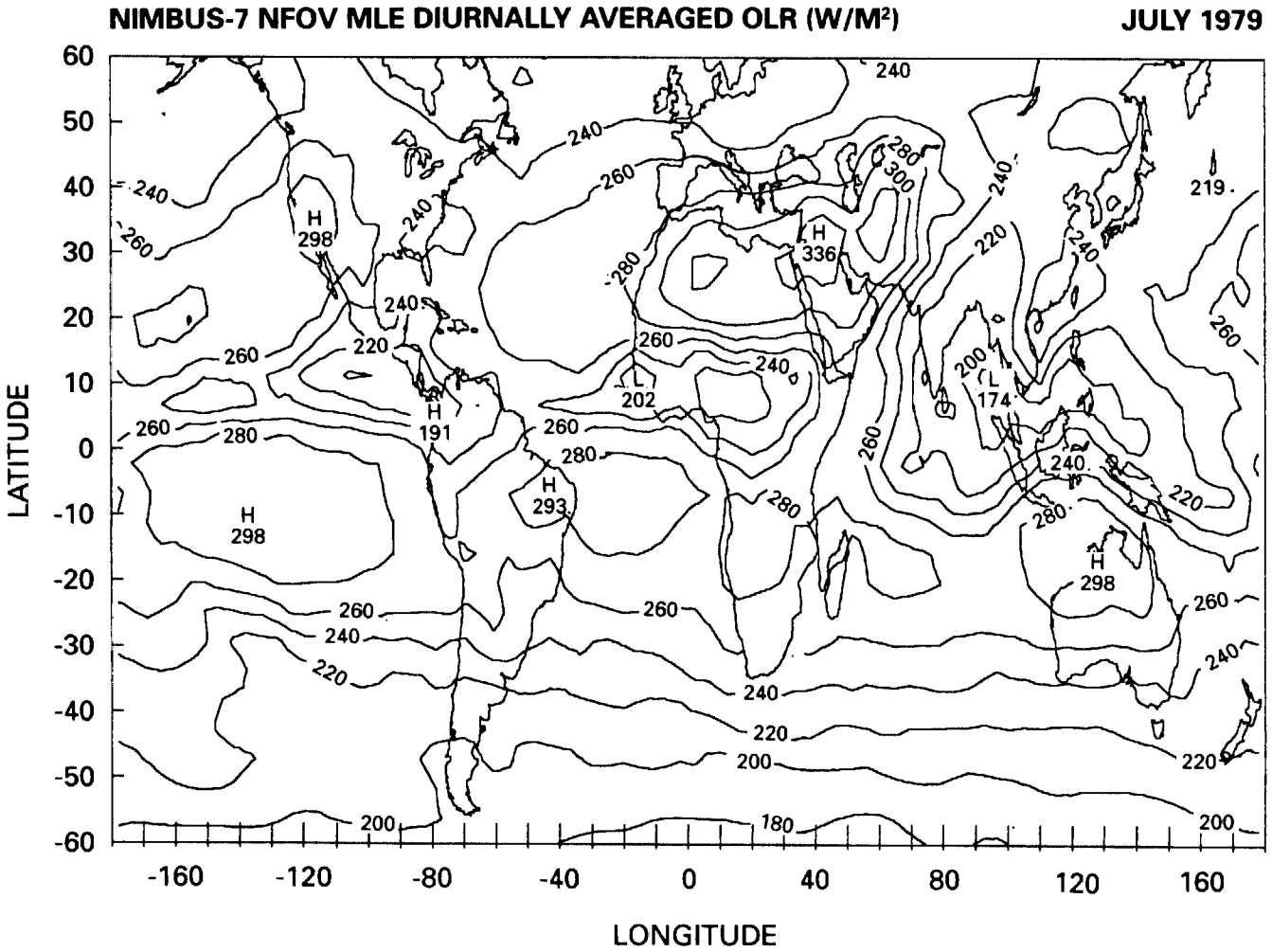

Figure 6-5. Monthly averaged outgoing longwave radiation for July 1979; MLCE algorithm results.

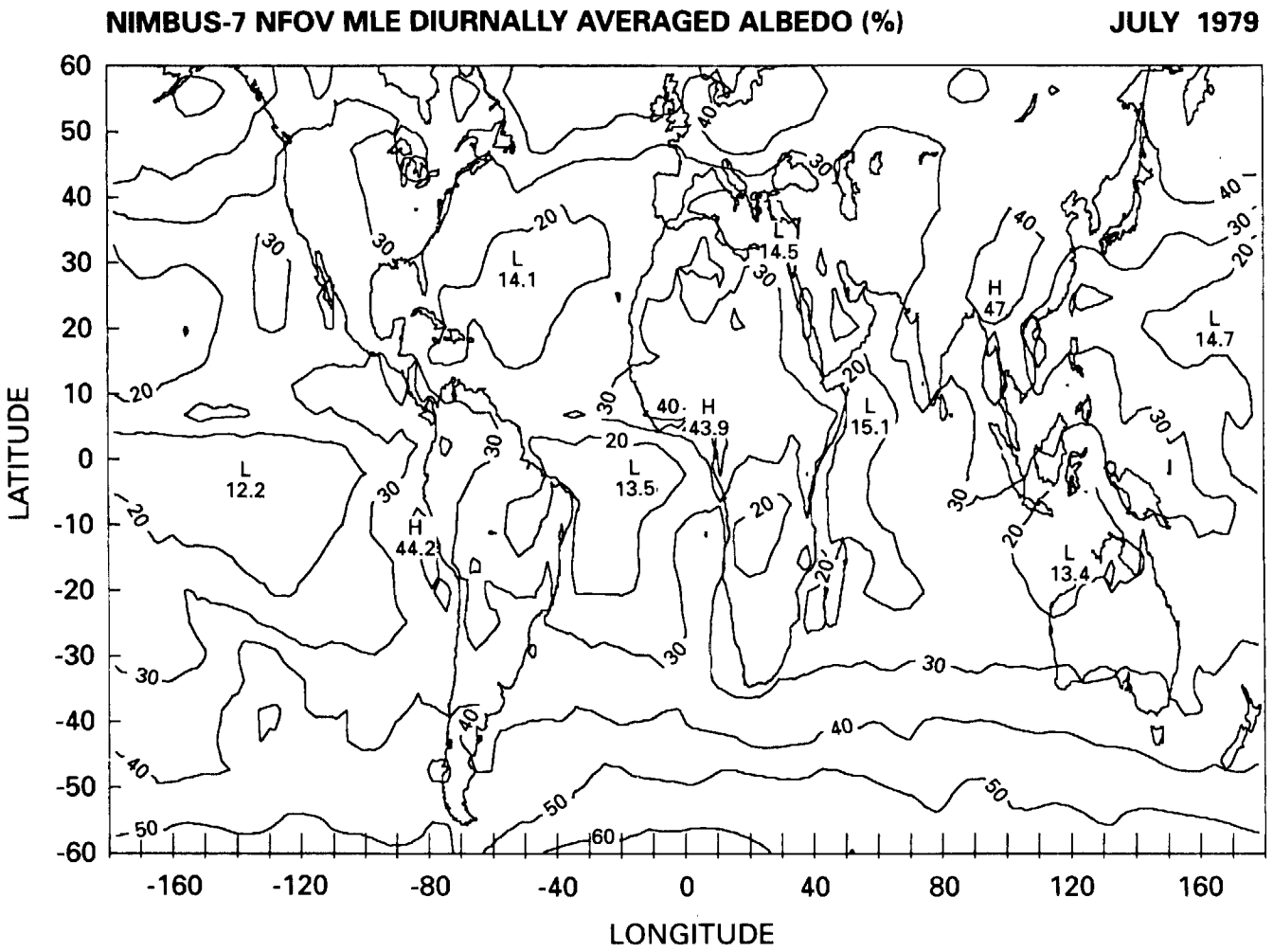

Figure 6-6. The July 1979 albedo; MLCE algorithm results.

7. THE SCENE RADIANCE TAPE (SRT)

7.1 INTRODUCTION

Nimbus-7 ERB scanner measurements for the period May 1979 through May 1980, were read from the ERB MATs, sorted by STA and satellite-viewing angle and stored on the SRTs as described in Section 2. The Earth is divided into 18,630 STAs which are roughly equal in area. At the Equator, an STA is 1.5° latitude by 1.5° longitude. The latitude dimension remains fixed, but the longitude increases with latitude and is 40° at the poles. Over each STA, the upward hemisphere is divided into 85 angular bins, but these are reduced to 49 bins by assuming symmetry about the (zenith/Sun) plane. Each 104-minute orbit begins and ends on the descending node (DN) near the subsatellite track crossing of the Equator at a time near local midnight. On the ascending node (AN), the satellite crosses the Equator near local noon.

For each orbit (ascending and descending nodes) longwave and shortwave radiance observations are collected and accumulated in their appropriate ERB STA and viewing angle bin. At the end of the orbit, the accumulated radiances are averaged. Because the Earth rotates slowly when compared to an orbital period, scenes observed on AN are different from those observed on DN. The result is that a greater subset of STAs are viewed during a single orbital pass, but with less angular coverage. The number of observations, and the variation about the mean is also recorded and written to magnetic tape for all locations and angular bins that were observed by the scanner.

The number of STA scenes and the number of angular bins that are viewed by the scanner for each orbit depends on the scan mode of the instrument (see Figure 2-1). The typical number of STA scenes and angular bins that are observed for the primary scan modes are shown in Table 7-1. In Table 7-2, the mean number of STA scenes and mean number of angular bins for each orbit are also provided. In general, between 4-6 thousand scenes are observed from 1-14 different angular views. Scan modes 3 and 4 provide the best angular sampling, while scan mode 5 gives the best spatial coverage. The scanner operated primarily in scan mode 5 from February 1979 through early September 1979, and exclusively in modes 3 and 4 from mid-September 1979 until the scanner failure on June 20, 1980.

The Scene-Radiance Tapes were processed for a continuous 13-month period from May 1979 through May 1980. The data set consists of a total of 39 tapes. Table 7-3 provides the NOPS sequence numbers for each tape along with the days of data that are available.

7.2 TAPE CHARACTERISTICS

An individual Scene-Radiance Tape (SRT) contains a standard 630-byte NOPS header, up to 8 days of sorted and averaged scanner radiance observations, and the standard NOPS Trailing Documentation File (TDF). All SRTs are 6,250 BPI and have a maximum of 10 files (NOPS header, 8 data days, and TDF). The data files are composed of numerous 28,200-byte physical record blocks. Each physical record contains 150 logical records (LRs) which are 188 bytes in length. An LR contains 1,504 bits (94 16-bit words). Each LR contains information about the average observed radiances for an individual ERB STA scene. The first five words in each LR

Table 7-1. The Mean Number of STA Scenes (bottom row) and the Percentage of STA Scenes (top row) Observed as a Function of the Number of Angular Bins Viewed for Different Scanner Operating Modes

The values shown are the averages for all orbits in the day.
Frequency distributions of the number of angular bins for an STA scene observed on an orbital basis

Number of Angular Bins																			
1	2	3	4	5	6	7	8	9	10	11	12	13	14	15	16	17	18	19	20
September 12, 1979 SCAN MODE: 1																			
24.4	22.0	12.0	7.1	5.5	4.2	3.7	3.9	4.2	4.3	3.9	2.7	1.4	0.5	0.2	0.1	0.0	0.0	0.0	0.0
1245.0	1122.0	613.0	362.0	281.0	214.0	188.0	197.0	217.0	219.0	198.0	135.0	70.0	27.0	8.0	3.0	1.0	0.0	0.0	0.0
September 16, 1979 SCAN MODE: 4																			
17.6	13.2	12.7	10.9	8.9	7.7	7.0	6.4	5.2	3.9	2.9	1.9	1.1	0.5	0.2	0.1	0.0	0.0	0.0	0.0
720.0	542.0	521.0	448.0	364.0	314.0	289.0	261.0	211.0	160.0	118.0	78.0	43.0	19.0	8.0	3.0	0.0	0.0	0.0	0.0
June 2, 1979 SCAN MODE: 5																			
27.3	22.3	15.0	10.5	7.1	4.6	3.8	3.1	2.5	1.7	0.9	0.4	0.6	0.0	0.0	0.0	0.0	0.0	0.0	0.0
1719.0	1407.0	947.0	659.0	444.0	291.0	240.0	198.0	159.0	110.0	58.0	25.0	40.0	2.0	0.0	0.0	0.0	0.0	0.0	0.0
December 26, 30, 1978; February 12, 1979 SCAN MODE: NADIR Position, None of the 4 telescopes points directly at nadir.																			
88.6	9.4	0.7	0.3	0.2	0.2	0.2	0.1	0.1	0.1	0.1	0.1	0.0	0.1	0.0	0.0	0.0	0.0	0.0	0.0
1108.0	117.0	8.0	3.0	2.0	2.0	2.0	2.0	1.0	1.0	1.0	1.0	1.0	1.0	0.0	0.0	0.0	0.0	0.0	0.0

Table 7-2. Mean Number of STA Scenes and Angular Bins/Scene Observed by the Nimbus-7 ERB Scanner as a Function of Operating Mode for Each Orbit

		Number of Angular Bins	
	Total Number of Scenes	Mean	Standard Deviation
Scan Mode - 1	5000	4.2	3.5
Scan Mode - 3/4	4100	4.9	3.3
Scan Mode - 5	6250	3.4	2.5
Nadir	1100	1.1	0.3

identify (1) the year; (2) the day of observation; (3) an Earth grid location, consisting of the zone number x 100 added to the relative TA number within the zone; (4) the sequential target number (1-2,070); and (5) the orbit number. The ERB scanner status, orbital node, and STA number are given in Word 9 and an LR continuation flag is indicated in Word 10. The remainder of the record contains radiance statistics and related satellite and solar parameters. The LR layout can accommodate up to 7 different angular views for each ERB STA. The mean number of angular views made by the ERB scanner on an orbit basis for an STA is generally less than 7 (see Tables 7-1 and 7-2), resulting in all information for a scene being located in one LR. If more than 7 angular views of an STA scene are recorded in an orbit, then a second LR follows. When this occurs, an LR continuation flag is set in a record to indicate that it contains information for the same STA scene as the previous record. If more than 14 different angular views for one STA scene are observed in an orbit, they are dropped from the processing and do not appear on the tape. This was found to occur very infrequently, less than 0.3% of the time as may be seen from Table 7-1. The structure of each LR is shown in Table 7-4.

7.3 TAPE LENGTH ESTIMATE

7.3.1 Data File Length

LOGICAL RECORD SIZE:	94 INTEGER*2 (16-bit) Words 188 bytes total
PHYSICAL RECORD SIZE:	150 LRs 28,200 bytes One inter-record gap (0.5-inch)
TAPE DENSITY:	6250 bpi 4.51 inches/PR
PHYSICAL RECORD LENGTH:	28,200 bytes/PR and interrecord gap 5.01 inches/PR
DATA FILE LENGTH ESTIMATE:	70,000 LRs (STA-scenes) 467 PRs (70,000 LR/150 LR/PR) 195 ft (467 PR * 5.01 inches/PR)

Table 7-3. List of Scene-Radiance Tapes Available from NSSDC

Month	NOPS Sequence No.	Total No. of Days	Data File Span	Calendar Days on Tape
May 1979	AN91211-1	8	2-9	1, 3-5, 7-9, 11
	AN91331-1	8	2-9	13-15, 17, 19-21, 23
	AN91441-1	6	2-7	24, 25, 27-29, 31
June 1979	AN91521-1	8	2-9	1, 2, 4-6, 8-10
	AN91631-1	8	2-9	12-14, 16-18, 20, 21
	AN91731-1	7	2-8	22, 24-26, 28-30
July 1979	AN91831-1	8	2-9	2-4, 6-8, 10, 11
	AN91931-1	8	2-9	12, 14-16, 18-20, 22
	AN92041-1	7	2-8	23, 24, 26-28, 30, 31
August 1979	AN92131-1	8	2-9	1, 3-5, 7-9, 11
	AN92241-1	8	2-9	12, 13, 15-17, 19-21
	AN92351-1	7	2-8	23-25, 27-29, 31
September 1979	AN92441-1	8	2-9	1, 2, 4-6, 8-10
	AN92551-1	8	2-9	12-14, 16-18, 20, 21
	AN92651-1	7	2-8	22, 24-26, 28-30
October 1979	AN92751-1	8	2-9	2-4, 6-8, 10, 11
	AN92851-1	8	2-9	12, 14-16, 18-20, 22
	AN92961-1	7	2-8	23, 24, 26-28, 30, 31
November 1979	AN93051-1	8	2-9	1, 3-5, 7-9, 11
	AN93161-1	8	2-9	12, 13, 15-17, 19-21
	AN93271-1	6	2-7	23-25, 27-29
December 1979	AN93351-1	8	2-9	1-3, 5, 7, 9-11
	AN93471-1	8	2-9	13-15, 17, 19, 21-23
	AN93591-1	6	2-7	25-27, 29-31
January 1980	AN00021-1	8	2-9	2-4, 6-8, 10, 11
	AN00121-1	8	2-9	12, 14-16, 18-20, 22
	AN00231-1	7	2-8	23, 24, 26-28, 30, 31
February 1980	AN00321-1	8	2-9	1, 3-5, 7-9, 11
	AN00431-1	8	2-9	12, 13, 15-17, 19-21
	AN00541-1	6	2-7	23-25, 27-29
March 1980	AN00621-1	8	2-9	2-4, 6-8, 10, 11
	AN00721-1	8	2-9	12, 14-16, 18-20, 22
	AN00831-1	7	2-8	23, 24, 26-28, 30, 31
April 1980	AN00921-1	8	2-9	1, 3, 5, 7-9, 11, 12
	AN01041-1	8	2-9	13, 15-17, 19-21, 23
	AN01151-1	5	2-6	24, 25, 27-29
May 1980	AN01221-1	8	2-9	1-3, 5-7, 9, 10
	AN01321-1	8	2-9	11, 13-15, 17-19, 21
	AN01431-1	8	2-9	22, 23, 25-27, 29-31

Table 7-4. NFOV Level-1 Scene-Radiance Tape Logical Data Record Format

WORD	MSB 32	LSB 1	BIT
1	YEAR (16)	JULIAN DAY OF YEAR (16)	32
2	CODED GRID LOCATION (16)	SEQUENTIAL-TA (16)	64
3	ORBIT NO. (16)	AVERAGE COSINE OF SOLAR ZENITH ANGLE (16)	96
4	TOTAL DAYLIGHT HOURS (16)	MEAN DAILY INSOLATION (16)	128
5	ERB SCANNER STATUS/ORB NODE/SUB-TA NO. (16)	LOGICAL RECORD CONTINUATION FLAG (16)	160
12	ANGULAR BIN NUMBERS (112)	LONGWAVE RADIANCE POPULATIONS (112)	384
19	SHORTWAVE RADIANCE POPULATIONS (112)	MEAN LONGWAVE RADIANCE (112)	608
26	MEAN SHORTWAVE RADIANCE (112)	MEAN BIDIRECTIONAL REFLECTANCE (112)	832
33	SUM OF SQUARES OF LONGWAVE RADIANCE OBSERVATIONS (224)		1056
40	SUM OF SQUARES OF BIDIRECTIONAL REFLECTANCES (224)		1280
47	AVERAGE RELATIVE AZIMUTH ANGLE (112)	AVERAGE SATELLITE ZENITH ANGLE (112)	1504

7.3.2 Tape Length Estimate

File	Estimate (FT)	Contents
1	0.1	2 630-byte NOPS headers
2-9	195	Approximately 70,000 STA scenes
10	0.5	Trailing Documentation File (7-9 630-byte records)
TOTAL:		1560.6 ft

7.4 PARAMETER DESCRIPTIONS

The descriptions of each parameter contained in the LR are summarized below:

Integer*2 Word Number	Parameter
1	Full Year
2	Julian Day
3	Coded TA (latitude zone x 100 + relative TA within a zone). ERB zones are 4.5° in latitude and counted from the South Pole. TAs are approximately equi-area regions spanning 4.5° x 4.5° latitude/longitude at the Equator. Within a zone, relative TAs are enumerated westward from Greenwich Meridian.
4	Sequential TA (1-2,070). TA number counted continuously from the South Pole to North Pole.
5	Orbit Number counted from launch date in 10/78
6	Average cosine of the solar zenith angle for the STA for all angular views (scaled by 10,000). Available only during hours of solar illumination.
7	Total sunlight hours (in half day) (scaled by 10)
8	Mean daily insolation at TA center (W/m^2 scaled by 10)
9	ERB scanner status/orbital node/sub-TA (1-9)

Units Digit:	(1)	Scanning in Mode 1
	(2)	Scanning in Mode 2
	(3)	Scanning in Mode 3
	(4)	Scanning in Mode 4
	(5)	Scanning in Mode 5
	(6)	Scanning is in nadir
Tens Digit:	(1)	Descending-Node
	(2)	Ascending-Node
Hundreds Digit:	(1-9)	STA Number

The scan status was obtained from the instrument status and scan information words located on the MAT for each major frame. This information was used to assign the scanner status for each STA scene according to the status of the first radiance observation in the orbit which falls in the STA.

10	LR continuation flag 0 - LR contains data for a different STA scene 9 - continuation of angular-bin data for the same STA scene as in the previous LR.

Each LR will contain up to seven different angular-bin views for an STA scene. If more angular-bin views are observed, then a second LR will follow with up to seven more angular-bin views for the same STA. This is noted by the appearance of a value of 9 in the LR continuation flag word of the second record. If more than 14 angular-bin views are observed for a single STA, then these will be excluded from the level-1 output tape. This has been determined to occur for less than 0.3% of the viewed scenes (see Table 7-1).

11-17	Angular-bin number (1-49) corresponding to a set of radiance observations in this sub-TA.
18-24	Longwave radiance population for each of seven angular-bin views
25-31	Shortwave radiance population for each of seven angular-bin views
32-38	Mean longwave radiance of the observations for each of 7 angular-bin views ($W/m^2/sr$ scaled by 100)
39-45	Mean shortwave radiance of the observations for each of 7 angular-bin views ($W/m^2/sr$ scaled by 100)
46-52	Mean bidirectional reflectance for each of 7 angular-bin views (sr^{-1} scaled by 10,000). Bidirectional reflectance is defined as the ratio of the observed shortwave radiance to the incoming insolation.
53-66	Sum of squares of longwave radiance observations for each of 7 angular-bin views ($(W/m^2/sr)^2$ scaled by 10) (32-bit words)
67-80	Sum of squares of bidirectional reflectances for each of 7 angular-bin views (sr^{-2} scaled by 10^7) (32-bit words)
81-87	Average relative azimuth angle observed for each of 7 angular-bin views (deg scaled by 100). Present only during daylight.
88-94	Average satellite zenith angle observed for each of 7 angular-bin views (deg scaled by 100). Present only during daylight.

7.5 SPECIAL NOTES

a. As indicated in Table 7-4, LRs consist almost exclusively of 16-bit data words. The two exceptions are the sums of squares of the longwave and shortwave radiances for a given scene and angular view. These parameter values routinely exceed the storage capacity of 2-byte signed integer words and are, therefore, stored as 4-byte integer words. These parameters occupy byte positions 129 through 184 in the LR.

b. When scaled by 100, the mean shortwave radiance for a scene and angular view occasionally exceeds the 32,767 maximum value of a 2-byte signed integer word. These values are stored, nevertheless, in the available 16 bits with the caveat that all 16 bits represent the magnitude of the number and its sign is positive. If the 2 bytes are interpreted as a conventional integer*2 FORTRAN word, a negative value results.

c. The ascending and descending node phases of an orbit are defined by the Z-component of the satellite velocity vector in an Earth-centered Cartesian coordinate system with positive Z-axis in the direction of the North Pole. Ascending node corresponds to a positive Z-component of velocity.

d. Missing or nonexistent data are indicated by the appearance of the fill value, zero. Following the last valid observation of an orbit, the remaining LRs of a physical record are 0-filled and readily noted by the 0 value obtained for the coded grid location in 2-byte integer word number 3 of the LR.

e. Angular parameters in the form of the cosine of the solar zenith angle, satellite zenith angle, and relative azimuth are not accumulated for a scene and angular bin for observations for which a shortwave radiance is unavailable. This includes all observations with solar zenith angles greater than 88° (i.e., little or no solar illumination) and daytime observations whose shortwave component was rejected during quality control checks. For these cases, some indication of the satellite geometry is still available in the angular bin numbers provided.

f. Mean daily insolation, 2-byte integer Word 8, is computed at the midpoint of the sequential TA (1-2,070) given in 2-byte integer Word 4.

8. THE SORTING INTO ANGULAR BINS (SAB) TAPE

8.1 DATA SET

A Sorting into Angular Bins (SAB) algorithm (see Section 3) has been used to process the Nimbus-7 ERB NFOV data set. Although the Nimbus-7 scanner operated for nearly 20 months, from November 16, 1978 to June 20, 1980, we have chosen to use this algorithm to produce a daily- and monthly-averaged Earth radiation budget for the 13-month period from May 1979 to May 1980. Because of poor sampling, primarily at night, the remaining months were not processed using this method. On a spatial scale, both 4.5° latitude zone and regional TA (i.e., approximately 500-km x 500-km grid elements) averages are derived, although sampling deficiencies limit the availability of the latter to monthly fields only. Observed zone and TA radiance populations within the 49 angular bins of the upwelling hemisphere (see Figure 2-3) are also given, as well as their means and standard deviations. Symmetry is assumed about the principal plane of the sun so that radiances viewed at the same satellite zenith angle, but at the opposite relative azimuths of $\pm\lambda$, are collected and averaged within a single bin. Ancillary data used in computing the ERB products are also provided. These include the scene classification of each ERB TA consisting of (a) the geographic composition (percentage of ocean, land, snow, and desert) and average total cloud cover of each target for bimonthly periods and (b) scene-dependent directional models used to convert the observed orbit-dependent albedo to a daily averaged parameter. These ERB products are provided on one 6,250-bpi magnetic tape which is available from the NSSDC located at the NASA/GSFC in Greenbelt, Maryland.

8.2 TAPE CHARACTERISTICS

The complete Nimbus-7 ERB NFOV SAB product data set is stored on a standard 6,250-bpi magnetic tape consisting of 15 files. The first file contains two standard NOPS header records. The next 13 files each contain one month of radiance statistics, Earth radiation budget products and ancillary data for all time and space scales. The last file contains a standard NOPS trailing documentation file (TDF), which provides the input tapes used to generate the SAB tape. An outline of the arrangement of the tape is provided in Table 8-1. The data product files (2 through 14) are composed of numerous 21,000-byte physical records, which are arranged in a chronological sequence of daily zonal data records, followed by the monthly zonal records and, finally, the monthly TA records. Each physical record contains 10 LRs of 2,100 bytes or, equivalently, 1,050 2-byte integer words. The first 2-byte word of each LR identifies the record type as either daily zonal, monthly zonal, or monthly TA. While these LRs contain equal amounts of occupied storage (i.e., 1,050 2-byte words), the zonal and TA records differ in the number of ERB parameters actually provided, and in the arrangement of the given parameters within the record. The internal structure of zonal records is shown in Table 8-2 and is the same for both daily and monthly averaging intervals. As indicated along the left edge of the table, these records contain 909 2-byte (454 1/2 4-byte) data values and 141 2-byte words of fill values. For monthly LRs, there are 523 2-byte data values and 527 2-byte fill values. Within both tables, the multiplicative factors used in producing the stored values are given for each parameter type, and within parentheses, the amount of storage (in bits) occupied by that parameter. Only monthly records exist for the individual TAs. The arrangement of the TA monthly record is described in Table 8-3. In Table 8-4 we provide an estimate of the length of the data files found on the SAB tape.

Table 8-1. Outline of ERB-7 NFOV SAB Product Tape	
File No.	Description
1	Two standard NOPS 630-byte header records
2	Daily and Monthly Products for May 1979
3	Daily and Monthly Products for June 1979
4	Daily and Monthly Products for July 1979
5	Daily and Monthly Products for August 1979
6	Daily and Monthly Products for September 1979
7	Daily and Monthly Products for October 1979
8	Daily and Monthly Products for November 1979
9	Daily and Monthly Products for December 1979
10	Daily and Monthly Products for January 1980
11	Daily and Monthly Products for February 1980
12	Daily and Monthly Products for March 1980
13	Daily and Monthly Products for April 1980
14	Daily and Monthly Products for May 1980
15	NOPS Trailing Documentation File consisting of copies of standard 630-byte NOPS header records from input tapes used to generate this output tape

8.3 TAPE LENGTH ESTIMATE

File	Estimate (FT)	Contents
1	0.1	2 630-byte records
2-14	98.8/file	40 LRs of daily-zonal data repeated for up to 24 data days in a month (24 days is the maximum number of days that the ERB instrument was ON for one month) 40 LRs containing monthly-zonal data 2,070 LRs containing monthly target-area data.
15	2.0	Trailing Documentation File (40, 630-byte records)
TOTAL:	1286.5 ft	

Table 8-2. ERB-7 NFOV SAB Product Tape Logical Data Record Format Zonal Daily Monthly Record

WORD	MSB 32		LSB 1	BIT
1	RECORD ID (16)	TIME SCALE (16)		32
2	DATA SPAN: YEAR, MONTH, DAY (16)	ZONE (16)		64
3	SPARE (16)	SPARE (16)		96
	SHORTWAVE RADIANCE POPULATIONS FOR 49 ANGULAR BINS (784)			880
52	MEAN SHORTWAVE RADIANCE FOR 49 ANGULAR BINS *10 (784)			1664
	ASCENDING-NODE LONGWAVE RADIANCE POPULATIONS FOR 49 ANGULAR BINS (784)			2448
101	MEAN ASCENDING-NODE LONGWAVE RADIANCE FOR 49 ANGULAR BINS *10 (784)			3232
	DESCENDING-NODE LONGWAVE RADIANCE POPULATIONS FOR 49 ANGULAR BINS (784)			4016
150	MEAN DESCENDING-NODE LONGWAVE RADIANCE FOR 49 ANGULAR BINS *10 (784)			4800
	STANDARD DEVIATION OF MEAN ASCENDING-NODE LONGWAVE RADIANCE FOR 49 ANGULAR BINS *100 (784)			5584
199	STANDARD DEVIATION OF MEAN DESCENDING-NODE LONGWAVE RADIANCE FOR 49 ANGULAR BINS *100 (784)			6368
	MEAN BIDIRECTIONAL REFLECTANCE FOR 49 ANGULAR BINS *1000 (784)			7152
248	STANDARD DEVIATION OF MEAN BIDIRECTIONAL REFLECTANCE FOR 49 ANGULAR BINS *10,000 (784)			7936
	POPULATION-WEIGHTED MEAN COSINE OF THE SOLAR ZENITH ANGLE FOR 49 ANGULAR BINS *10,000 (784)			8720
297	MAXIMUM COSINE SOLAR ZENITH ANGLE FOR 49 ANGULAR BINS *10,000 (784)			9504
	MINIMUM COSINE SOLAR ZENITH ANGLE FOR 49 ANGULAR BINS *10,000 (784)			10288
346	STANDARD DEVIATION COSINE SOLAR ZENITH ANGLE FOR 49 ANGULAR BINS *10,000 (784)			11072
	MEAN COSINE SOLAR ZENITH ANGLE FOR 49 ANGULAR BINS *10,000 (784)			11856
395	NUMBER OF STA SCENES OBSERVED FOR ASCENDING-NODE LONGWAVE FOR 49 ANGULAR BINS (784)			12640
	NUMBER OF STA SCENES OBSERVED FOR DESCENDING-NODE LONGWAVE FOR 49 ANGULAR BINS (784)			13424
444	NUMBER OF STA SCENES OBSERVED FOR SHORTWAVE FOR 49 ANGULAR BINS (784)			14208
445	AVERAGE ASCENDING-NODE LONGWAVE FLUX *10 (16)	AVERAGE DESCENDING-NODE LONGWAVE FLUX *10 (16)		14240
446	DAILY-AVERAGE LONGWAVE FLUX *10 (16)	AVERAGE SATELLITE-OBSERVED SHORTWAVE FLUX *10 (16)		14272
447	AVERAGE SATELLITE OBSERVED ALBEDO *10 (16)	DAILY-AVERAGED ALBEDO *10 (16)		14304
448	NET RADIATION *10 (16)	AVERAGE SOLAR INSOLATION *10 (16)		14336
449	AVERAGE NUMBER DAYLIGHT HOURS *10 (16)	AVERAGE COSINE SOLAR ZENITH ANGLE *10,000 (16)		14368
450	DAILY-AVERAGED SHORTWAVE FLUX *10 (16)	SPARE (16)		14400
451	ERBE DIRECTIONAL MODEL COEFFICIENTS-x^3 *1000 (16)	ERBE DIRECTIONAL MODEL COEFFICIENTS-x^2 *1000 (16)		14432
452	ERBE DIRECTIONAL MODEL COEFFICIENTS-X *1000 (16)	ERBE DIRECTIONAL MODEL COEFFICIENTS-OFFSET *1000 (16)		14464
453	GEOGRAPHY: PERCENT OCEAN *10 (16)	GEOGRAPHY: PERCENT LAND *10 (16)		14496
454	GEOGRAPHY: PERCENT SNOW *10 (16)	GEOGRAPHY: PERCENT DESERT *10 (16)		14528
455	GEOGRAPHY: PERCENT CLOUD-COVER *10 (16)	FILL (16)		14560
525	FILL (2240)			16800

Table 8-3. ERB-7 NFOV SAB Product Tape Logical Data Record Format TA Monthly Record

WORD	MSB 32		LSB 1	BIT
1	RECORD ID (16)	TIME SCALE (16)		32
2	DATA SPAN: YEAR, MONTH (16)	SEQUENTIAL TA (16)		64
3	SPARE (16)	SPARE (16)		96
	DAILY-AVERAGED SHORTWAVE RADIANCE POPULATIONS FOR 49 ANGULAR BINS (784)			880
52	DAILY-AVERAGED ASCENDING-NODE LONGWAVE RADIANCE POPULATIONS FOR 49 ANGULAR BINS (784)			1664
	DAILY-AVERAGED ASCENDING-NODE POPULATION WEIGHTED LONGWAVE RADIANCE FOR 49 ANGULAR BINS *10 (784)			2448
101	DAILY-AVERAGED DESCENDING-NODE LONGWAVE RADIANCE POPULATIONS FOR 49 ANGULAR BINS (784)			3232
	DAILY-AVERAGED DESCENDING-NODE POPULATION-WEIGHTED LONGWAVE RADIANCE FOR 49 ANGULAR BINS *10 (784)			4016
150	STANDARD DEVIATION OF DAILY-AVERAGED ASCENDING-NODE LONGWAVE RADIANCE FOR 49 ANGULAR BINS *100 (784)			4800
	STANDARD DEVIATION OF DAILY-AVERAGED DESCENDING-NODE LONGWAVE RADIANCE FOR 49 ANGULAR BINS *100 (784)			5584
199	DAILY-AVERAGED POPULATION-WEIGHTED BIDIRECTIONAL REFLECTANCE FOR 49 ANGULAR BINS *1000 (784)			6368
	STANDARD DEVIATION OF DAILY-AVERAGED BIDIRECTIONAL REFLECTANCE FOR 49 ANGULAR BINS *10,000 (784)			7152
248	DAILY-AVERAGED POPULATION-WEIGHTED MEAN COSINE OF THE SOLAR ZENITH ANGLE FOR 49 ANGULAR BINS *10,000 (784)			7936
249	AVERAGE ASCENDING NODE LONGWAVE FLUX * 10 (16)	DAILY AVERAGE DESCENDING NODE LONGWAVE FLUX *10 (16)		7968
250	DAILY-AVERAGE LONGWAVE FLUX *10 (16)	AVERAGE SHORTWAVE FLUX *10 (16)		8000
251	DAILY-AVERAGED ALBEDO *10 (16)	NET RADIATION *10 (16)		8032
252	AVERAGE SOLAR INSOLATION *10 (16)		AVERAGE NUMBER DAYLIGHT HOURS *10 (16)	8064
253	AVERAGE COSINE SOLAR ZENITH ANGLE *10,000 (16)		ERBE DIRECTIONAL MODEL COEFFICIENTS-X^3 *1000 DAYS 1-15 (16)	8096
254	ERBE DIRECTIONAL MODEL COEFFICIENTS-X^2 *1000 DAYS 1-15 (16)		ERBE DIRECTIONAL MODEL COEFFICIENTS-X *1000 DAYS 1-15 (16)	8128
255	ERBE DIRECTIONAL MODEL COEFFICIENTS-OFFSET *1000 DAYS 1-15 (16)		GEOGRAPHY: PERCENT OCEAN *10 DAYS 1-15 (16)	8160
256	GEOGRAPHY: PERCENT LAND *10 DAYS 1-15 (16)		GEOGRAPHY: PERCENT SNOW *10 DAYS 1-15 (16)	8192
257	GEOGRAPHY: PERCENT DESERT *10 DAYS 1-15 (16)		GEOGRAPHY: PERCENT CLOUD-COVER *10 DAYS 1-15 (16)	8224
258	ERBE DIRECTIONAL MODEL COEFFICIENTS-X^3 *1000 DAYS 16-31 (16)		ERBE DIRECTIONAL MODEL COEFFICIENTS-X^2 *1000 DAYS 16-31 (16)	8256
259	ERBE DIRECTIONAL MODEL COEFFICIENTS-X *1000 DAYS 16-31 (16)		ERBE DIRECTIONAL MODEL COEFFICIENTS-OFFSET *1000 DAYS 16-31 (16)	8288
260	GEOGRAPHY: PERCENT OCEAN *10 DAYS 16-31 (16)		GEOGRAPHY: PERCENT LAND *10 DAYS 16-31 (16)	8320
261	GEOGRAPHY: PERCENT SNOW *10 DAYS 16-31 (16)		GEOGRAPHY: PERCENT DESERT *10 DAYS 16-31 (16)	8352
262	GEOGRAPHY: PERCENT CLOUD-COVER *10 DAYS 16-31		FILL (16)	8384
525	FILL (8416)			16800

Table 8-4. ERB NFOV SAB Data File Length Estimate	
LOGICAL RECORD SIZE:	1,050 INTEGER*2 (16-bit) Words 2,100 bytes total
PHYSICAL RECORD SIZE:	10 Logical Records 21,000 bytes One inter-record gap (0.5-inch)
TAPE DENSITY:	6,250 bpi 3.86 inches/PR
PHYSICAL RECORD LENGTH:	21,000 bytes/PR /6,250 bytes/inch + 0.5 inch
ESTIMATE OF NUMBER OF LOGICAL RECORDS:	40 (zones) * 24 (# days) + 40 (zones, monthly) + 2,070 (TA, monthly) = 3,070 LR's = ~ 307 PR's
FILE LENGTH ESTIMATE:	98.8 ft (307 PR's * 3.86 inches/PR)

8.4 PARAMETER DESCRIPTION

8.4.1 Record Identifiers

Each LR is described by the first 16-bit integer word as follows:

- 11 = Zonal-Daily Record
- 12 = Zonal-Monthly Record
- 13 = Target-Area Monthly Record

The time scale of each LR is described in the second 16-bit word as follows:

- 1 = Daily Record
- 2 = Monthly Record

The day, month, and year of each LR is given in the third 16-bit word as follows:

DATA SPAN = (DAY OF MONTH)*1000 + MONTH (01=JAN)*10 + YEAR

where

YEAR = 9 FOR 1979
YEAR = 0 FOR 1980

For monthly records, the day value is set to zero.

8.4.2 Earth Radiation Budget Data

Parameter values are given, in general, for both TA and 4.5° zonal band resolution. Among these are longwave and shortwave radiances, M ($W/m^2/sr$ scaled by 10), longwave and

shortwave fluxes, F (W/m^2 scaled by 10), solar insolation, I (W/m^2 scaled by 10), albedo a (% scaled by 10), and bidirectional reflectance $\rho = M/I$ (sr^{-1} scaled by 1,000).

8.4.2.1 *Daily Zonal Band Data*

As a function of the 49 satellite zenith and relative azimuth bins of Figure 2-3, the following parameters are provided:

Daily ascending node shortwave radiance population
Daily ascending node longwave radiance population
Daily descending node longwave radiance population
Daily averaged population weighted shortwave radiance
Daily averaged ascending node population weighted longwave radiance
Daily averaged descending node population weighted longwave radiance
Standard deviation of the daily ascending node longwave radiance
Standard deviation of the daily descending node longwave radiances
Standard deviation of the daily ascending node bidirectional reflectances
Daily averaged population weighted cosine of the solar zenith angle
Daily averaged population weighted bidirectional reflectance
Daily averaged solar insolation
Average number of daylight hours in the half-day
Daily statistics for the cosine of the solar zenith angle: (1) standard deviation of the mean, (2) maximum cosine, (3) minimum cosine, and (4) the mean determined by weighting the cosine from a scene equally with all other scenes. An individual scene is defined as a STA region (there are nine equal area regions in each ERB TA shown in Figure 1) when viewed from one ascending or descending node orbital pass.
The number of individual scenes observed by the ERB scanner for daytime longwave, nighttime longwave, and shortwave observations

As a function of 4.5° zones only without further subdivision into viewing angle bins, we have

Average ascending node longwave flux
Average descending node longwave flux
Daily average (ascending and descending) longwave flux
Average shortwave flux
Daily averaged shortwave flux
Average satellite observed albedo
Daily averaged (diurnally adjusted) albedo
Net radiation
Average solar insolation
Average number of daylight hours in the half day
Average cosine of the solar zenith angle
ERBE directional model (DM): the DM is described using a cubic polynomial of four zonal coefficients ($a_3 \ldots a_o$). The coefficients form an equation which is evaluated as a function of the cosine of the solar zenith angle (X) as follows:

$$DM = a_3X^3 + a_2X^2 + a_1X + a_o$$

Scene classification: surface composition in percent areal coverage of ocean, land, snow, desert, and percent total cloud cover. In deriving diurnal models, the cloud coverage is assumed to be distributed uniformly throughout the zonal band.

8.4.2.2 *Monthly Zonal Band Data*

The parameters provided in the monthly 4.5° zonal record are identical to those for the zonal daily record, with the following exceptions:

- No radiance data (filled)
- No directional models (filled)
- No geography or cloud coverage percentage (filled)

Monthly mean fluxes are determined by averaging daily estimates obtained during ERB-on days rather than, by contrast, integrating monthly mean radiances over the 49 angular bins. Monthly averaged radiance statistics can be computed, if desired, from the individual daily averages provided on this tape.

8.4.2.3 *Monthly Target Area Data*

The parameters provided in the monthly TA records are summarized below. As a function of the 49 satellite zenith and relative azimuth bins shown in Figure 2-3, the following parameters are given:

Daily averaged shortwave radiance population
Daily averaged ascending node longwave radiance population
Daily averaged descending node longwave radiance population
Daily averaged ascending node population weighted longwave radiance
Daily averaged descending node population weighted longwave radiance
Standard deviation of the daily ascending node longwave radiances
Standard deviation of the daily descending node longwave radiances
Standard deviation of the daily ascending node bidirectional reflectances
Daily averaged population weighted cosine of the solar zenith angle
Daily averaged population weighted bidirectional reflectance

The following parameters are provided by TA only:

Average number of daylight hours in the half-day
Average ascending node longwave flux
Average descending node longwave flux
Daily averaged (ascending and descending) longwave flux
Daily averaged shortwave flux
Daily averaged (diurnally adjusted) albedo
Net radiation
Average solar insolation
Average cosine of the solar zenith angle

ERBE directional model (DM): the DM is described using a cubic polynomial of four coefficients ($a_3 \ldots a_o$) for the TA. The coefficients form an equation that can be evaluated as a function of the cosine of the solar zenith angle (X) as follows:

$$DM = a_3X^3 + a_2X^2 + a_1X + a_o$$

Scene classification: surface composition in percent areal coverage of ocean, land, snow, desert, and percent total cloud cover. In deriving directional models, cloud coverage is assumed to be distributed uniformly over each surface type with the TA.

8.4.3 Explanation of Fill Values

In most instances, a fill value of zero is used to indicate missing or unavailable data. The exceptions are as follows:

- Zonal Daily/Monthly Data
  - Minimum cosine solar zenith angle for 49 angular bins (filled with +10,000)
  - All fluxes and albedos (filled with -10,000)
  - Net radiation, average solar insolation, and average number of daylight hours (filled with -10,000)
  - Average STA cosine solar zenith angle not subdivided into angular bin (filled with 22,222)
- Target Area Monthly Data
  - All fluxes and albedos (filled with -10,000)
  - Net radiation, average solar insolation, and average number of daylight hours (filled with -10,000)
  - Average cosine solar zenith angle (filled with 22,222)

9. THE MAXIMUM LIKELIHOOD CLOUD ESTIMATION TAPE

9.1 THE DATA SET

An MLCE algorithm has been used to process the Earth Radiation Budget (ERB) NFOV data set. Although the ERB-7 scanner operated for nearly 20 months from November 16, 1978 through June 20, 1980, we have chosen to apply this algorithm to data collected only over the 13-month period from May 1979 to May 1980. Prior to May 1979, there were extended periods when the scanner observations interfered with the short-lived LIMS, and measurements, therefore, were not taken. The resulting NFOV data set for these months is very sparse, especially on descending node, and is not included in the final MLCE data product. The input radiance data were taken from the SRT data set. The resulting Earth radiation budget products, cloud data, and associated statistics are stored on five 6,250-bpi magnetic tapes, which are available from the National Space Science Data Center, located at the Goddard Space Flight Center in Greenbelt, Maryland.

Earth radiation budget products have been produced by the MLCE algorithm at several spatial and temporal scales and separately for all sky and clear sky conditions by combining parameter estimates from individual observations into lower resolution time and space average. Daily and monthly averages are available at STA resolution (166 km)^2 and at TA resolution (500 km)^2. Daily averages are also given for 40 4.5° latitude zones. In a second averaging procedure, ERB products are subdivided not only by spatial and temporal scale, but also as a function of satellite viewing angle bin (see Figure 2-3). Daily parameter values are provided for this method for the 40 latitude zones. Further details of the averaging schemes used for both methods are presented below.

9.1.1 Subtarget Area (STA) Data

The ERB world grid consists of 2,070 TAs of approximately equal area. These regions are further partitioned into 9 STAs. These form a 3 x 3 grid within each TA and are numbered 1 to 9, beginning at the southeast corner (see Section 2). Daily and monthly means are available at STA resolution. Unless otherwise stated, monthly STA averages are derived from sums of daily STA averages (see Section 9.3.2.5).

9.1.2 Target Area Data

Daily and monthly average data are also available on a TA basis. Most daily average TA data are derived from daily average STA data (see Section 9.3.2.2). That is

$$\overline{TA_j} = \frac{1}{9}\sum_{n=1}^{9} \overline{STA_{j,n}}$$

where $\overline{TA_j}$ is the daily average for the jth TA, $\overline{STA_{j,n}}$ represents the daily STA average for each of 9 subtargets within the jth TA, and it is assumed that each STA has a value. In actual processing, averages are formed for each TA that has at least one STA filled with data. Monthly means are computed using the same arithmetic averaging technique from STA monthly means.

9.1.3 Zonal Data

ERB parameters and statistics are also collected and averaged over 4.5° latitude zones. Most zonal daily means are computed from STA daily means in the following way (see Section 9.3.2.3):

$$\overline{Z_j} = \frac{1}{N}\sum_{n-1}^{N} \overline{STA_n}$$

where $\overline{Z}_j$ is the daily average for zone j, $\overline{STA}_n$ represents the daily STA average for the nth sub-target within the jth latitude zone, and N is the total number of STA values used in the computation.

9.1.4 Zonal and Angular-Bin Data

A second method of presenting daily zonal average data is to sort the ERB products, cloud data, and associated statistics into 49 discrete satellite-viewing angle bins as shown in Figure 2-3. Satellite relative azimuth angles of 180° to 360° are grouped with their symmetric counterpart across the principle plane of the Sun to form eight relative azimuth angle bins. Observations falling in the outermost zenith angle ring (bins 42-49) were not processed (see Section 4). Zonal and angular-bin averages were formed in the following way:

$$\overline{ZAB_{j,k}} = \frac{1}{N}\sum_{n-1}^{N} X_{j,k}$$

where $\overline{ZAB}_{j,k}$ is the daily average product for latitude zone j and angular bin k, $X_{j,k}$ is a single flux or other MLCE product for the same zone and angular bin, and N is the total daily population in zone j and bin k.

9.2 TAPE CHARACTERISTICS

The Nimbus-7 ERB NFOV MLE product data set is stored on five standard 6,250-bpi magnetic tapes. Each tape contains three months of data. The 13th month of data exists alone on the fifth tape. The first file of each tape contains two standard NOPS header records. This is followed by the data files, one for each ERB-ON day of the month, plus an additional monthly average file. This sequence of data files is repeated for the remaining months of data contained on the tape. An outline of the arrangement of the first tape is provided as an example in Table 9-1.

The data files consist of numerous 4,156-byte physical record blocks. The LRs are the same size (i.e., each physical record contains only one LR). Each LR contains 2,078 16-bit integer words for a total of 33,248 bits. The first eight words give the time resolution (i.e., monthly or daily) and type (i.e., subtarget, target, zonal, or zonal angular bin) of the data values along with a coded parameter number, STA number (if not applicable, set to 0), data scale factor, and the day (if not applicable, set to 0), month, and year. STA and TA data are given on both a daily and monthly basis, while zonal and zonal angular-bin data appear only as daily averages. Tables 9-2

Table 9-1. Outline of a Typical ERB-7 NFOV MLE Product Tape

File No.	Description
1	Two standard NOPS 630-byte header records
2-23	Daily products for May 1979
24	Monthly products for May 1979
25-47	Daily products for June 1979
48	Monthly products for June 1979
49-71	Daily products for July 1979
72	Monthly products for July 1979

Table 9-2. ERB-7 NFOV MLE Product Tape Logical Record Format for STA Data

Word			Bit
1	Time Scale (16)	Data Type (16)	32
3	Parameter Number (16)	STA Number (16)	64
5	Scale Factor (16)	Calendar Day of Month (16)	96
7	Month (16)	Year (16)	128
9-2078	Data described by the parameter number in word 3 for the STA named in word 4 for each of 2070 target areas. (For monthly data, calendar day = 0).		33248

through 9-5 show the arrangements of LRs for the four data types. Table 9-6 defines the data parameter corresponding to each coded parameter number; availability in time, space, and angular bin categories; and the scale factor applied. Longwave and shortwave fluxes, net radiation, insolation, and standard deviation are given in W/m^2 scaled by 10; albedo and fractional cloud coverage categories (i.e., clear, partly, mostly, and overcast) are in percent scaled by 100; and day observation rates are scaled by 100. Within a file, the STA records appear first, followed in order by the TA, zonal and zonal bin records.

9.3 PARAMETER DESCRIPTION

9.3.1 Record Identifiers

Each LR is described by the first eight 16-bit words as follows:

Word 1-Time Scale
- 1 = daily
- 2 = monthly

Word 2-Data Type
- 11 = daily STA
- 12 = daily TA
- 13 = daily zonal
- 14 = daily zonal angular bin
- 21 = monthly STA
- 22 = monthly TA

Word 3-Coded Parameter Number: See Table 9-6 for a summary of parameter numbers and the corresponding data descriptions

Word 4-STA No.: A number from 1-9 locating the data within a particular TA (set to 0 for TA, zonal, zonal angular bin data)

Word 5-Scale Factor: The integer number by which the value in stated physical units is multiplied

Word 6-Calendar Day of Month: 1-31 (set to 0 for monthly data)

Word 7-Month of Year: 1-12

Word 8-Year: 1979 or 1980

9.3.2 Earth Radiation Budget Data

The Earth radiation budget parameters and associated data within each data type are described in detail in Sections 9.3.2.1 through 9.3.2.6.

Table 9-3. ERB-7 NFOV MLE Product Tape Logical Record Format for TA Data

Word			Bit
1	Time Scale (16)	Data Type (16)	32
3	Parameter Number (16)	STA Number (16)	64
5	Scale Factor (16)	Calendar Day of Month (16)	96
7	Month (16)	Year (16)	128
9-2078	Data described by the parameter number in word 3 for each of 2070 target areas. (STA number = 0 and calendar day = 0 for monthly data.)		33248

Table 9-4. ERB-7 NFOV MLE Product Tape Logical Record Format for Zonal Data

Word			Bit
1	Time Scale (16)	Data Type (16)	32
3	Parameter Number (16)	STA Number (16)	64
5	Scale Factor (16)	Calendar Day of Month (16)	96
7	Month (16)	Year (16)	128
9-48	Data described by the parameter number in word 3 for each of 40 latitude zones. (STA number and calendar day = 0.)		768
49-2078	Fill		33248

Table 9-5. ERB-7 NFOV MLE Product Tape Logical Record Format for Zonal Angular-Bin Data

Word			Bit
1	Time Scale (16)	Data Type (16)	32
3	Parameter Number (16)	STA Number (16)	64
5	Scale Factor (16)	Calendar Day of Month (16)	96
7	Month (16)	Year (16)	128
9-48	Data described by the parameter number in word 3 for zones 1-40 for angular bin 1 (STA and calendar day = 0.)		768
49-88	Same as above for angular bin 2		1408
89-1968	Same as above for angular bins 3-49		31488
1969-2078	Fill		33248

Table 9-6. Parameter List

Parameter No.	Description	Time and Spatial Coverage	Scale Factor
1	AN Longwave Flux	STA & TA - D&M, ZN & ZNBN - D	10
2	DN Longwave Flux	STA & TA - D&M, ZN & ZNBN - D	10
3	Avg. Longwave Flux	STA & TA - D&M, ZN & ZNBN - D	10
4	AN Shortwave Flux	STA & TA - D&M, ZN & ZNBN - D	10
5	Net Radiation	STA & TA - D&M, ZN & ZNBN - D	10
6	Observed Albedo	STA & TA - D&M, ZN & ZNBN - D	100
7	Corrected Albedo	STA & TA - D&M, ZN & ZNBN - D	100
8	Standard Deviation of AN Longwave Flux	STA - D&M, ZNBN -D	10
9	Standard Deviation of DN Longwave Flux	STA - D&M, ZNBN -D	10
10	Standard Deviation of AN Shortwave Flux	STA - D&M, ZNBN -D	10
11	AN LW Population	STA - D, ZNBN - D	1
12	DN LW Population	STA - D, ZNBN - D	1
13	AN SW Population	STA - D, ZNBN - D	1
14	No. Days of Month Observed-AN LW	STA & TA - M	1
15	No. Days of Month Observed-DN LW	STA & TA - M	1
16	No. Days of Month Observed-AN SW	STA & TA - M	1
17	Avg. No. of Days of Month Observed/STA Within Each TA-AN LW	TA - M	100

STA = Subtarget Area Average
TA = Target Area Average
ZN = Zonal Average
ZNBN = Zonal and Angular-Bin Average

D = Daily Average
M = Monthly Average
AN = Ascending Node
DN = Descending Node

Table 9-6. Parameter List

Parameter No.	Description	Time and Spatial Coverage	Scale Factor
18	Avg. No. of Days of Month Observed/STA Within Each TA-DN LW	TA - M	100
19	Avg. No. of Days of Month Observed/STA Within Each TA-AN SW	TA - M	100
20-38	Same Sequence as Above but Data for Clear Skies Only		
39	Solar Insolation	ZN - D	10
40	AN% Obs. Clear Sky	TA & ZNBN - D, TA - M	100
41	AN% Obs. Partly Cloudy	TA & ZNBN - D, TA - M	100
42	AN% Obs. Mostly Cloudy	TA & ZNBN - D, TA - M	100
43	AN% Obs. Overcast	TA & ZNBN - D, TA - M	100
44	DN% Obs. Clear Sky	TA & ZNBN - D, TA - M	100
45	DN% Obs. Partly Cloudy	TA & ZNBN - D, TA - M	100
46	DN% Obs. Mostly Cloudy	TA & ZNBN - D, TA - M	100
47	DN% Obs. Overcast	TA & ZNBN - D, TA - M	100
48	AN Ersatz Clear Sky Longwave Flux	TA - D	10
49	DN Ersatz Clear Sky Longwave Flux	TA - D	10
50	AN Ersatz Clear Sky Obs. Albedo	TA - D	100

STA = Subtarget Area Average
TA = Target Area Average
ZN = Zonal Average
ZNBN = Zonal and Angular-Bin Average

D = Daily Average
M = Monthly Average
AN = Ascending Node
DN = Descending Node

9.3.2.1 STA Daily Average Data

The following is a list of parameters which are available on a daily STA basis. Along with a description of each quantity is the coded parameter number, given separately for clear and all-sky cloud conditions, found in Word 3 of each LR. The units of flux are (W/m^2), the albedo is in percent.

Coded Parameter No. All Sky	Clear Sky	Description
1	20	AN longwave flux
2	21	DN longwave flux
3	22	Average longwave flux (computed from parameters 1 and 2 or 20 and 21 is available; otherwise, fill value)
4	23	AN shortwave flux
5	24	Net radiation (computed from parameters 3 and 7 or 22 and 26, along with the daily average solar insolation if available; otherwise, fill value). If parameter 7, 26, or the daily average solar insolation is unavailable for subtargets in or near the polar night, then the net radiation becomes the negative of parameter 3 or 22.
6	25	AN observed albedo
7	26	AN diurnally corrected albedo
8	27	Standard deviation of AN longwave fluxes
9	28	Standard deviation of DN longwave fluxes
10	29	Standard deviation of AN shortwave fluxes
11	30	AN longwave flux population (number of views per day)
12	31	DN longwave flux population (number of views per day)
13	32	AN shortwave flux population (number of views per day)

9.3.2.2 TA Daily Average Data

The following is a list of parameters which are available on a daily TA basis. Along with a description of each quantity is the parameter number, given separately for clear and all-sky conditions, found in Word 3 of each LR. Unless otherwise indicated, TA averages are computed from daily STA averages. The units of flux are (W/m^2), the albedo is in percent.

Coded Parameter No. All Sky	Clear Sky	Description
1	20	AN longwave flux
2	21	DN longwave flux
3	22	Average longwave flux (computed from parameters 1 and 2 or 20 and 21 if available; otherwise, fill value)
4	23	AN shortwave flux
5	24	Net radiation (computed from parameters 3 and 7 or 22 and 26, along with the daily average solar insolation if all are available; otherwise,

		fill value). If the daily average solar insolation is zero, or very small and parameters 7 or 26 are unavailable, for TA in or near the polar night, then the net radiation becomes the negative of parameter 3 or 22.
6	25	AN observed albedo
7	26	AN diurnally corrected albedo

Cloud Data
(Cloud category data are collected over entire TA)

40		AN % observations clear
41		AN % observations partly cloudy
42		AN % observations mostly cloudy
43		AN % observations overcast
44		DN % observations clear
45		DN % observations partly cloudy
46		DN % observations mostly cloudy
47		DN % observations overcast

Ersatz Clear-Sky Parameters

A secondary method of obtaining daily average TA clear-sky estimates of ascending- and descending-node longwave fluxes and ascending-node observed albedos is utilized. An average of the first five observations within a TA (regardless of sky condition) is obtained. The next observation is compared to this average. If it is larger (in the case of fluxes) or smaller (in the case of albedo), then a new average is formed in the following way:

$$NewAvg = \frac{(4 \times OldAvg) + LastObs}{5}$$

The new average is calculated each time an observation is larger (smaller) than the current average. The units of flux are W/m^2; the albedo is in percent.

Parameter No.		
All Sky	Clear Sky	Description
48		AN ersatz clear-sky longwave flux
49		DN ersatz clear-sky longwave flux
50		AN ersatz clear-sky albedo

9.3.2.3 Zonal Daily Average Data

The following is a list of parameters that are available on a daily zonal-band basis. Along with a description of each quantity is the parameter number, given separately for clear- and all-sky cloud conditions, found in Word 3 of each LR. Unless otherwise indicated, zonal averages are computed from daily STA averages. The units of flux are W/m^2; the albedo is in percent.

Parameter No. All Sky	Clear Sky	Description
1	20	AN longwave flux
2	21	DN longwave flux
3	22	Average longwave flux (computed from parameters 1 and 2 or 20 and 21 if both of a pair are available; otherwise, fill value)
4	23	AN shortwave flux
5	24	Net radiation (computed from parameters 3 and 7 or 22 and 26 along with the daily average solar insolation if available; otherwise, fill value). If latitude zones in or near the polar night, then the net radiation becomes the negative of parameter 3 or 22.
6	25	AN observed albedo
7	26	AN diurnally corrected albedo
39		Solar insolation
		Cloud Data (Zonal Cloud Category Frequencies are computed from TA cloud category frequencies)
40		AN % observations clear
41		AN % observations partly cloudy
42		AN % observations mostly cloudy
43		AN % observations overcast
44		DN % observations clear
45		DN % observations partly cloudy
46		DN % observations mostly cloudy
47		DN % observations overcast

9.3.2.4 Zonal Angular Bin Daily Average Data

The following is a list of parameters which have been grouped or averaged by latitude zones and by satellite-viewing angle bins. Along with a description of each quantity is the parameter number, given separately for clear- and all-sky cloud conditions, found in Word 3 of each LR. The units of flux are W/m^2; the albedo is in percent.

Parameter No. All Sky	Clear Sky	Description
1	20	AN longwave flux
2	21	DN longwave flux
3	22	Average longwave flux (computed from parameters 1 and 2 or 20 and 21 if both of a pair are available; otherwise, fill value)
4	23	AN shortwave flux
5	24	Net radiation (computed from parameters 3 and 7 or 22 and 26, along with the daily average solar insolation if available; otherwise, fill value). If the daily average insolation is zero, or very small and

		parameters 7 and 26 are unavailable, then the net radiation becomes the negative of parameter 3 or 22 for latitude zones in or near the polar night.
6	25	AN observed albedo
7	26	AN diurnally corrected albedo
8	27	Standard deviation of AN longwave fluxes
9	28	Standard deviation of DN longwave fluxes
10	29	Standard deviation of AN shortwave fluxes
11	30	AN longwave flux population
12	31	DN longwave flux population
13	32	AN shortwave flux population
		Cloud Data
40		AN % observations clear
41		AN % observations partly cloudy
42		AN % observations mostly cloudy
43		AN % observations overcast
44		DN % observations clear
45		DN % observations partly cloudy
46		DN % observations mostly cloudy
47		DN % observations overcast

9.3.2.5 STA Monthly Average Data

The following is a list of parameters that are available on a monthly STA basis. Along with a description of each quantity is the parameter number, given separately for clear- and all-sky cloud conditions, found in Word 3 of each LR. Unless otherwise indicated, monthly averages have been calculated from daily averages. The units of flux are W/m^2; the albedo is in percent.

Parameter No. All Sky	Clear Sky	Description
1	20	AN longwave flux
2	21	DN longwave flux
3	22	Average longwave flux (computed from parameters 1 and 2 or 20 and 21 if available; otherwise, fill value)
4	23	AN shortwave flux
5	24	Net radiation
6	25	AN observed albedo
7	26	AN diurnally corrected albedo
8	27	Standard deviation of daily average AN longwave fluxes
9	28	Standard deviation of daily average DN longwave fluxes
10	29	Standard deviation of daily average AN shortwave fluxes
14	33	Number of days with AN longwave flux data
15	34	Number of days with DN longwave flux data
16	35	Number of days with AN shortwave flux data

9.3.2.6 TA Monthly Average Data

The following is a list of parameters that are available on a monthly TA basis. Along with a description of each quantity is the parameter number, given separately for clear- and all-sky cloud conditions, found in Word 3 of each LR. Unless otherwise indicated, monthly averages are calculated from monthly STA averages. The units of flux are W/m^2; the albedo is in percent.

Parameter No. All Sky	Clear Sky	Description
1	20	AN longwave flux
2	21	DN longwave flux
3	22	Average longwave flux (computed from parameters 1 and 2 or 20 and 21 if available; otherwise, fill value)
4	23	AN shortwave flux
5	24	Net radiation
6	25	AN observed albedo
7	26	AN diurnally corrected albedo
14	33	Number of days with AN longwave flux data
15	34	Number of days with DN longwave flux data
16	35	Number of days with AN shortwave flux data
17	36	Average number of days with AN longwave flux data per STA (within each TA)
18	37	Average number of days with DN longwave flux data per STA (within each TA)
19	38	Average number of days with AN shortwave flux data per STA (within each TA)
		Cloud Data (Monthly cloud category frequencies are computed from daily cloud category frequencies)
40		AN % observations clear
41		AN % observations partly cloudy
42		AN % observations mostly cloudy
43		AN % observations overcast
44		DN % observations clear
45		DN % observations partly cloudy
46		DN % observations mostly cloudy
47		DN % observations overcast

9.3.3 Units and Fill Values

All values of longwave and shortwave flux, net radiation, standard deviation, and solar insolation have units of watts per square meter (W/m^2). All values of albedo, diurnally corrected albedo, and cloud category frequency are expressed in percent (%).

Fill values denoting missing or unavailable data are set to -10,000 for all parameters. If, for example, a particular TA was not viewed during any orbit of a particular day, then all fluxes, standard deviations, populations, cloud category frequencies, etc., would have a value of -10,000. If this TA was viewed under overcast sky conditions only, however, then only clear-sky parameters would have fill values. Note that for this second condition, the percent overcast category would be 100, while the percent partly cloudy, mostly cloudy, and clear categories would be 0 and not -10,000. Shortwave fluxes, solar insolation, and albedos beyond the terminator region also have values of -10,000.

REFERENCES

Ardanuy, P. E., L. L. Stowe, A. Gruber, M. Weiss, and C. S. Long, 1988, "Longwave Cloud Radiative Forcing as Determined From Nimbus-7 Observations," *J. Climate*, 2, pp. 766-799.

Arking, A. and S. K. Vemury, 1984, "The Nimbus-7 ERB Data Set: A Critical Analyses," *J. Geophys. Res.*, 89, pp. 5089-5097.

Brooks, D. R., E. F. Harrison, P. Minnis, J. T. Suttles, and R. S. Kandel, 1986, "Development of Algorithms for Understanding the Temporal and Spatial Variability of the Earth's Radiation Balance," *Rev. Geophys.*, 24, pp. 422-438.

Brooks, D. R. and M. A. Fenn, 1988a, *Summary of Along-Track Data From the Earth Radiation Budget Satellite for Several Major Desert Regions*, NASA RP-1197, 144 pages.

Brooks, D. R. and M. A. Fenn, 1988b, *Summary of Along-Track Data From the Earth Radiation Budget Satellite for Several Representative Ocean Regions*, NASA RP-1206, 213 pages.

Hartmann, D. L., V. Ramanathan, A. Berroir, and G. E. Hunt, 1986, "Earth Radiation Budget Data and Climate Research," *Rev. Geophys. Space Phys.*, 24, pp. 439-468.

Jacobowitz, H., H. V. Soule, H. L. Kyle, F. B. House, and the Nimbus-7 ERB Experiment Team, 1984a, "The Earth Radiation Budget (ERB) Experiment: An Overview," *J. Geophys. Res.*, 89, pp. 5021-5038.

Jacobowitz, H., and R. J. Tighe, and the Nimbus-7 ERB Experiment Team, 1984b, "The Earth Radiation Budget Derived From the Nimbus-7 ERB Experiment," *J. Geophys Res.*, 89, pp. 4997-5010.

Kyle, H. L., Ardanuy, P. E., and E. J. Hurley, 1985, "The Status of the Nimbus-7 ERB Earth Radiation Budget Data Set," *Bull. Amer. Meteor. Soc.*, 66, pp. 1378-1388.

Kyle, H. L., K. L. Vasanth, and the Nimbus-7 ERB Experiment Team, 1986, "Some Characteristic Differences in the Earth's Radiation Budget Over Land and Ocean Derived From the Nimbus-7 ERB Experiment," *J. Climate Appl. Meteor.*, 25, pp. 958-981.

Kyle, H. L., A. Mecherikunnel, P. Ardanuy, L. Penn, B. Groveman, G. Campbell, and T. H. Vonder Haar, 1990, "A Comparison of Two Major Earth Radiation Budget Data Sets," *J. Geophys. Res.*, (in press).

Ramanathan, V., 1987, "The Role of Earth Radiation Budget Studies in Climate and General Circulation Research," *J. Geophys. Res.*, 92, pp. 4075-4095.

Ramanathan, V., R. D. Cess, E. F. Harrison, P. Minnis, B. R. Barkstrom, E. Ahmad, and D. Hartman, 1989a, "Cloud-Radiative Forcing and Climate Insights From the Earth Radiation Budget Experiment," *Science*, 243, pp. 57-63.

Ramanathan, V., B. R. Barkstrom, and E. F. Harrison, 1989b, "Climate and the Earth's Radiation Budget," *Physics Today*, 42, pp. 22-32.

Raschke, E., T. H. Vonder Haar, M. Pasternak, and W. R. Bandeen, 1973, *The Radiation Balance of the Earth-Atmosphere System From Nimbus-3 Radiation Measurements*, NASA TN D-7249, 73 pages.

Smith, E. A., and M. R. Smith, 1987, "Interannual Variability of the Tropical Radiation Balance and the Role of Extended Cloud Systems," *J. Atmos. Sci.*, 44, pp. 3210-3234.

Smith, G. L., R. N. Green, E. Raschke, K. M. Avis, J. T. Suttles, B. A. Wielicki, and R. Davies, 1986, "Inversion Methods for Satellite Studies of the Earth's Radiation Budget: Development of Algorithms for the ERBE Mission," *Rev. Geophys.*, 24, pp. 407-421.

Stowe, L. L., C. G. Wellemeyer, T. F. Eck, H. Y. M. Yeh, and the Nimbus-7 Cloud Data Processing Team, 1988, "Nimbus-7 Global Cloud Climatology, Part I: Algorithms and Validation," *J. Climate*, 1, pp. 445-470.

Stowe, L. L., H. Y. M. Yeh, T. F. Eck, C. G. Wellemeyer, H. L. Kyle, and the Nimbus-7 Cloud Data Processing Team, 1989, "Nimbus-7 Global Cloud Climatology, Part II: First Year Results," *J. Climate*, 2, pp. 671-709.

Suttles, J. T., R. N. Green, P. Minnis, G. L. Smith, W. F. Staylor, B. A. Wielicki, I. J. Walker, D. F. Young, V. R. Taylor, and L. L. Stowe, 1988, *Angular Radiation Models for the Earth-Atmosphere System, Volume I: Shortwave Radiation*, NASA RP-1184, Volume I, 144 pages.

Suttles, J. T., R. N. Green, G. L. Smith, B. A. Wielicki, I. J. Walker, V. R. Taylor, and L. L. Stowe, 1989, *Angular Radiation Models for the Earth-Atmosphere System, Volume II: Longwave Radiation*, NASA RP-1184, Vol. II, 84 pages.

Taylor, V. R. and L. L. Stowe, 1984, "Reflectance Characteristics of Uniform Earth and Cloud Surface Derived From Nimbus-7 ERB," *J. Geophys. Res.*, 89, pp. 4987-4996.

Vemury, S. K. L. Stowe, and H. Jacobowitz, 1984, "Sample Size and Scene Identification (Cloud) Effect on Albedo," *J. Geophys. Res.*, 89, pp. 5345-5353.

Wielicki, B. A., and R. N. Green, 1989, "Cloud Identification for ERBE Radiative Flux Retrieval," *J. Appl. Meteor.*, 28, pp. 1131-1146.

ACRONYMS, ABBREVIATIONS, AND SYMBOLS

ADM	angle dependent model
AN	ascending node
C	centigrade
CAT	Calibration Adjustment Table
deg	degree
DM	directional model
DN	descending node
ERB	Earth Radiation Budget
ERBE	Earth Radiation Budget Experiment
km	kilometer
LIMS	Limb Infrared Monitor of the Stratosphere
LR	logical record
LW	longwave
m	meter
MAT	Master Archive Tape
MLCE	Maximum Likelihood Cloud Estimation
MLE	Maximum Likelihood Estimation
N	north
NASA	National Aeronautics and Space Administration
NFOV	Narrow-Field-of-View
NSSDC	National Space Science Data Center
NW	northwest

OLR	Outgoing Longwave Radiation
PR	physical record
S	south
SAB	Sorting into Angular Bins
SE	southeast
SR	steradian
SRT	Scene Radiance Tape
STA	Sub-Target Area
SW	shortwave
TA	target area
TOA	top of the atmosphere
W	watts
WFOV	Wide-Field-of-View

NASA National Aeronautics and Space Administration

Report Documentation Page

1. Report No.	2. Government Accession No.	3. Recipient's Catalog No.
NASA RP-1246		

4. Title and Subtitle
User's Guide: Nimbus-7 Earth Radiation Budget Narrow-Field-of-View Products.
Scene Radiance Tape Products, Sorting Into Angular Bins Products, and Maximum Likelihood Cloud Estimation Products

5. Report Date
November 1990

6. Performing Organization Code
936

7. Author(s)
H. Lee Kyle, Richard R. Hucek, Brian Groveman, and Richard Frey

8. Performing Organization Report No.
90B00143

10. Work Unit No.

9. Performing Organization Name and Address
Goddard Space Flight Center
Greenbelt, MD 20771

11. Contract or Grant No.
NAS5-29373

13. Type of Report and Period Covered
Reference Publication

12. Sponsoring Agency Name and Address
National Aeronautics and Space Administration
Washington, DC 20546-0001

14. Sponsoring Agency Code

15. Supplementary Notes
H. Lee Kyle: Goddard Space Flight Center, Greenbelt, MD; Richard R. Hucek, Brian Groveman (now affiliated with Computer Sciences Corporation), and Richard Frey (now affiliated with SMSRC): Research and Data Systems Corporation, Greenbelt, MD

16. Abstract
The archived Earth radiation budget products produced from the Nimbus-7 ERB narrow-field-of-view scanner are described. The principal products are broadband outgoing longwave radiation (4.5 μm to 50 μm), reflected solar radiation (0.2 μm to 4.8 μm), and the net radiation. Daily and monthly averages are presented on a fixed global equal area, $(500\ km)^2$, grid for the period May 1979 to May 1980. Two independent algorithms are used to estimate the outgoing fluxes from the observed radiances. The algorithms are described and the results compared. The products are divided into three subsets: the Scene Radiance Tapes (SRT) contain the calibrated radiances; the Sorting into Angular Bins (SAB) tape contains the SAB produced shortwave, longwave, and net radiation products; and the Maximum Likelihood Cloud Estimation (MLCE) tapes contain the MLCE products. The tape formats are described in detail.

17. Key Words (Suggested by Author(s))	18. Distribution Statement
Earth radiation budget, Nimbus-7, Bidirectional Reflectances, Earth albedo, outgoing longwave radiation	Unclassified - Unlimited Subject Category 47

19. Security Classif. (of this report)	20. Security Classif. (of this page)	21. No. of pages	22. Price
Unclassified	Unclassified	80	A05